



# Observation and modelling of ozone-destructive halogen chemistry in a passive degassing volcanic plume

Luke Surl<sup>1,2</sup>, Tjarda Roberts<sup>1</sup>, and Slimane Bekki<sup>2</sup>

<sup>1</sup>CNRS, Laboratoire de Physique et de Chimie de l'Environnement et de l'Espace, Université d'Orléans, Orléans, France

<sup>2</sup>LATMOS/IPSL, Sorbonne Université, UVSQ, CNRS, Paris, France

**Correspondence:** Luke Surl (luke.surl@cnrs-orleans.fr)

## Abstract.

Volcanoes emit halogens into the atmosphere that undergo chemical cycling in plumes and cause destruction of ozone. The impacts of volcanic halogens are inherently difficult to measure at volcanoes, and the complexity of the chemistry, coupled with the mixing and dispersion of the plume, makes the system challenging to model numerically.

5 We present aircraft observations of the Mount Etna plume in the summer of 2012, when the volcano was passively degassing. Measurements of SO<sub>2</sub> — an indicator of plume intensity — and ozone were made in the plume a few 10s of km from the source, revealing a strong negative correlation between ozone and SO<sub>2</sub> levels. From these observations we estimate a mean in-plume ozone loss rate of  $1.3 \times 10^{-5}$  molecules of O<sub>3</sub> per second per molecule of SO<sub>2</sub>. This value is similar to observation-derived estimates reported very close to the Mount Etna vents, indicating continual ozone loss in the plume up to at least 10's km  
10 downwind.

The chemically reactive plume is simulated using a new numerical 3D model “WRF-Chem Volcano” (WCV), a version of WRF-Chem we have modified to incorporate volcanic emissions (including HBr and HCl) and multi-phase halogen chemistry. We used nested grids to model the plume close to the volcano at 1 km. The focus is on the early evolution of passively degassing plumes aged less than one hour and up to 10's km downwind.

15 The model reproduces the so-called ‘bromine explosion’: the daytime bromine activation process by which HBr in the plume is converted to other more reactive forms that continuously cycle in the plume. These forms include the radical BrO, a species whose ratio with SO<sub>2</sub> is commonly measured in volcanic plumes as an indicator of halogen ozone-destroying chemistry. We track the modelled partitioning of bromine between its forms. The model yields in-plume BrO/SO<sub>2</sub> ratios (around 10<sup>-4</sup> mol/mol) similar to those observed previously in Etna plumes. The modelled BrO/SO<sub>2</sub> is lower in plumes which are more  
20 dilute (e.g. at greater windspeed). It is also slightly lower in plumes in the middle of the day compared than in the morning and evening, due to BrO's reaction with diurnally varying HO<sub>2</sub>. Sensitivity simulations confirm the importance of near-vent products from high temperature chemistry, notably bromine radicals, in initiating the ambient temperature plume halogen cycling. Note also that heterogeneous reactions that activate bromine also activate a small fraction of the emitted chlorine; the resulting production of chlorine radical Cl causes a strong reduction in the methane lifetime and increasing formation of  
25 HCHO in the plume.



Modelled rates of ozone depletion are found to be similar to those derived from aircraft observations. Ozone destruction in the model is controlled by the processes that recycle bromine, with about three-quarters of this recycling occurring via reactions between halogen oxide radicals. Through sensitivity simulations, a relationship between the magnitude of halogen emissions and ozone loss is established.

30 Volcanic halogens cycling impacts profoundly the overall plume chemistry, notably hydrogen oxide radicals ( $\text{HO}_x$ ), nitrogen oxides ( $\text{NO}_x$ ), sulfur, and mercury chemistry. In the model, it depletes  $\text{HO}_x$  within the plume, increasing the lifetime of  $\text{SO}_2$  and hence slowing sulfate aerosol formation. Halogen chemistry also promotes the conversion of  $\text{NO}_x$  into nitric acid ( $\text{HNO}_3$ ). This, along with the displacement of nitrate out of background aerosols in the plume, results in enhance  $\text{HNO}_3$  levels and an almost total depletion of  $\text{NO}_x$  in the plume. The halogen-mercury model scheme is simple but includes newly-identified  
35 photo-reductions of mercury halides. With this set-up, the mercury oxidation is found to be slow and in near-balance with the photo-reduction in the plume. Overall, the model findings demonstrate that halogen chemistry has to be considered for a complete understanding of sulfur,  $\text{HO}_x$ , reactive nitrogen, and mercury chemistry, and of the formation of sulfate particles in volcanic plumes.

## 1 Introduction

### 40 1.1 Background

Volcanoes emit mixtures of various gases and particulates into the atmosphere. Of the gaseous emissions,  $\text{H}_2\text{O}$ ,  $\text{CO}_2$ , and  $\text{SO}_2$  are the species with the greatest fluxes. Most studies on the atmospheric impact of volcanic emissions have focused on sulfur because of its well-known effects on atmospheric composition, notably aerosol loading and climate (e.g. Oppenheimer et al., 2011). Several other species are emitted from volcanoes, including the primary focus of this study: halogens. Chlorine, bromine,  
45 and fluorine are routinely detected in various proportions within volcanic plumes, and are emitted primarily as hydrogen halides. Gerlach (2004) reported that gaseous emissions from arc volcanoes are, on average, 0.84%  $\text{HCl}$ , 0.061%  $\text{HF}$ , and 0.0025%  $\text{HBr}$ . Iodine has also been detected in volcanic plumes (e.g. Aiuppa et al., 2005; Bobrowski et al., 2017), but its emission fluxes are typically about two orders of magnitude below those of bromine.

The quantities of halogen species emitted from a volcano and their temporal variability appear to provide information on sub-  
50 surface processes (Pyle and Mather, 2009). Correlations between the bromine-to-sulfur ratio and volcanic activity have been found in long-term observations (e.g. Bobrowski and Giuffrida, 2012; Dinger et al., 2018; Warnach et al., 2019), suggesting that this ratio could potentially be used for monitoring and forecasting of volcanic activity. However, volcanic halogen emissions are not just potential indicators of sub-surface processes. Importantly, they impact the chemical composition of the atmosphere and hence possibly the climate. For instance ozone, the precursor of the most important atmospheric oxidant (the hydrogen  
55 oxide radical  $\text{OH}$ ), is found to be greatly depleted in volcanic plumes containing halogens (Rose et al., 2006; Vance et al., 2010; Kelly et al., 2013; Surl et al., 2015). Ozone is predominately destroyed by bromine chemistry cycles (Bobrowski et al., 2007; von Glasow, 2010; Roberts, 2018). Halogen chemistry also leads to the depletion of nitrogen oxides ( $\text{NO}_x$ ) and hydrogen oxide radicals ( $\text{HO}_x$ ) (Bobrowski et al., 2007; Roberts et al., 2009; Jourdain et al., 2016). and may oxidise mercury to more soluble,



and therefore more easily deposited, forms (von Glasow, 2010). The effects are not limited to the troposphere because volcanic  
60 plumes can also reach the tropopause region (Rose et al., 2006; Millard et al., 2006; Lurton et al., 2018), sometimes injecting  
halogens directly into the stratosphere. In the case of bromine-rich eruptions, this could result in massive stratospheric ozone  
depletion, dependent upon the fraction of emitted halogens that avoid dry- and wet-removal processes within the tropospheric  
plume and are therefore able to reach the stratosphere (Kutterolf et al., 2013; Cadoux et al., 2015; Brenna et al., 2020).

All these impacts of volcanic halogens depend critically on the extent of the conversion of emitted volcanic hydrogen halides  
65 into halogen radicals, a process called halogen activation. Indeed, hydrogen halides are weakly reactive and very soluble. As  
the result, their direct impact on atmospheric chemistry is very limited and short-lived because they are rapidly removed from  
the atmosphere. In contrast, halogen radicals are much more reactive chemically, in particular with respect to ozone, and  
less soluble. Therefore, assessing the atmospheric impacts of volcanic halogens requires a quantitative understanding of the  
physico-chemical plume processes driving the partitioning of volcanic halogen species, especially bromine species, between  
70 radicals and hydrogen halides. This is the primary focus of the present study. Note that only a small fraction of chlorine  
emissions undertakes reactive chemistry in plumes, and this small fraction is mostly activated as a result of bromine chemistry  
(Rüdiger et al., 2020, and references therein). As in most studies on volcanic plume halogen chemistry, fluorine and iodine are  
ignored. The solubility and stability of HF, the main emitted fluorine species, are such that no significant fluorine chemistry  
occurs within the plume (von Glasow et al., 2009). Iodine, while very reactive, is of substantially lower in-plume abundance  
75 than bromine and chlorine (Aiuppa et al., 2005).

Once emitted at high temperatures in the atmosphere, volcanic volatiles are cooled very quickly by the fast mixing of the  
plume with the surrounding air. Whilst some halogen radicals, as well as HO<sub>x</sub> and NO<sub>x</sub>, may be formed by high-temperature re-  
actions immediately after emission from the vent (in the so-called “effective source region” see Bobrowski et al., 2007; Roberts  
et al., 2019, and references therein), it is the atmospheric chemistry in the cooled and expanding plume that causes a sustained  
80 halogen cycling that impacts tropospheric ozone. This halogen chemistry continues to occur as the plume disperses into the  
background atmosphere. This chemistry is complex and non-linear. The major bromine cycling driving bromine activation and  
ozone loss is shown in Figure 1. Heterogeneous processes involving acidic aerosol are the main pathway by which HBr is con-  
verted to reactive forms. The complete cycle requires photolysis reactions and therefore only occurs within the daytime. This  
bromine cycle is sometimes referred to as the “bromine explosion” (Wennberg, 1999; Bobrowski et al., 2007) because of its  
85 autocatalytic nature; bromine extracted from HBr can continue to cycle and generate further reactive bromine from this source.  
Although no equivalent “chlorine explosion” exists, heterogeneous reactions can also generate reactive chlorine radicals (via  
BrCl) which can react with ozone to form chlorine oxide species.

A fast interchange exists between Br and BrO. The Br + O<sub>3</sub> → BrO + O<sub>2</sub> reaction consumes an O<sub>3</sub> molecule, while BrO  
photolysis effectively reverses this as the O radical produced quickly reacts with O<sub>2</sub> to form O<sub>3</sub>. When BrO is reduced to Br  
90 via any other pathway (directly or indirectly), the net result is the loss of an O<sub>3</sub> molecule.

As well as depleting ozone, halogen chemistry has influences on other chemical systems, such as through reactions with NO<sub>x</sub>  
and HO<sub>x</sub> as shown in Figure 1. Volcanic halogens deplete HO<sub>x</sub>, increasing the lifetime of SO<sub>2</sub> with respect to OH oxidation,  
and oxidation of CH<sub>4</sub> by Cl radicals can reduce significantly the in-plume lifetime of CH<sub>4</sub> (Jourdain et al., 2016).

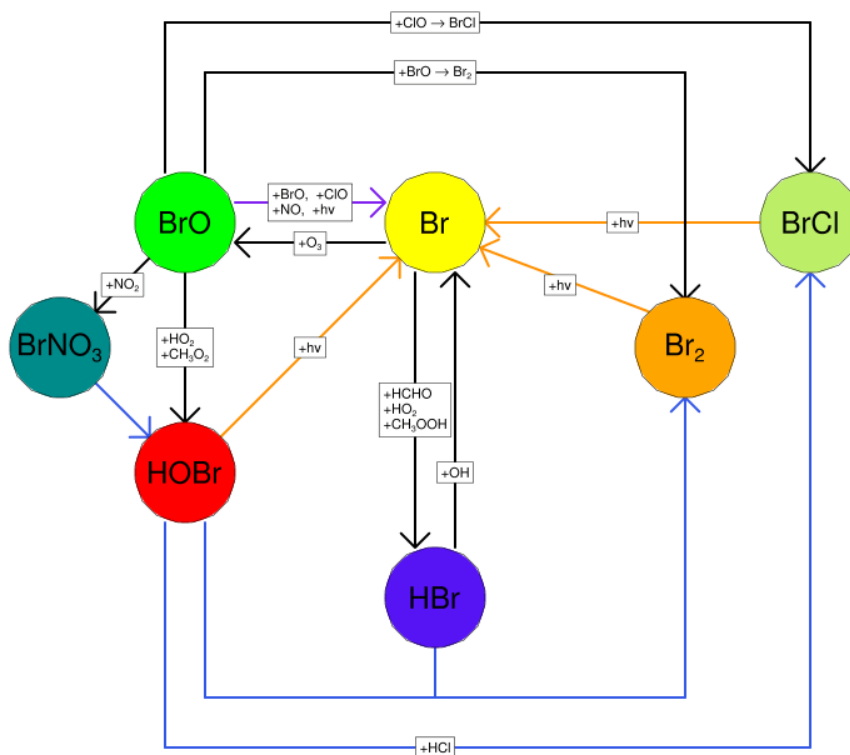


**Figure 1.** The major reactions of the bromine cycle. Orange lines indicate photolysis reactions, blue lines heterogeneous reactions, black lines other gas phase reactions.  $\text{BrO} \rightarrow \text{Br}$  includes one photolysis reaction and three other reactions.

Jourdain et al. (2016) modelled Ambrym plume and found halogens' depletive effect on  $\text{HO}_x$  to further increase the lifetime of  $\text{SO}_2$  with respect to oxidation by OH by 36%, and that Cl radicals reduced the in-plume lifetime of  $\text{CH}_4$ . Modelling by Roberts et al. (2009) indicates that volcanic halogen chemistry can result in conversion of in-plume  $\text{NO}_x$  to  $\text{HNO}_3$ .

Finally, volcanoes are also sources of mercury to the atmosphere (Pyle and Mather, 2003) mainly in the inert form  $\text{Hg}(0)$  (Witt et al., 2008; Bagnato et al., 2007). A 1D model study by von Glasow (2010) suggested that this mercury could be rapidly oxidised by halogen chemistry in a volcanic plume to more soluble forms, easily removed from the atmosphere (Seigneur and Lohman, 2008). Significant advances in understanding of the kinetics of halogen-mercury chemistry have been made in the last decade (e.g. Saiz-Lopez et al., 2018, 2019) and these are included in the modelling part of this study.

## 1.2 Observation and modelling studies

The current understanding of halogen chemistry within volcanic plumes is based upon a body of observations that have used a variety of techniques, coupled with numerical modelling results, most of which have used zero- or one-dimensional chemical box models.



### 1.2.1 Observations

There are two main methods for measuring halogens in volcanic plumes, remote sensing and in-situ sampling.

Remote sensing accounts for most observations of reactive halogens in volcanic plumes. Since the first reported detection by Bobrowski et al. (2003), bromine monoxide (BrO) has been observed within the plume of dozens of volcanoes by differential optical absorption spectroscopy (DOAS) (see Gutmann et al. (2018) for a recent catalogue of such observations). A smaller number of measurements of in-plume ClO and OClO have also been reported. These halogen molecules have spectroscopic signatures within the ultraviolet range, meaning they can be identified from the same data that is used to monitor SO<sub>2</sub>, including data collected from long-term DOAS monitoring networks at volcanoes (Dinger et al., 2018; Warnach et al., 2019). As well as ground and airbourne observations, BrO has been observed in the plumes of some larger volcanic eruptions by satellite-based instruments (e.g. Hörmann et al., 2013; Seo et al., 2019), though such large eruptions are the focus of a future study rather than this one.

In-situ sampling of halogens provides the most direct approach to quantify total halogen emissions: time-averaged sampling has for decades been used to quantify total volcanic halogen emission contents for F, Cl, Br and I (e.g. Aiuppa et al. (2004); Wittmer et al. (2014)). Modern techniques now allow for a degree of speciation in the bromine observed through these methods (Rüdiger et al., 2017, 2020). For most reactive halogen species, these methods required samples to be collected in-situ and then subsequently analysed in-lab. Consequently, there are fewer in-situ observations of reactive halogens than by remote sensing.

As well as these direct approaches, ozone measurements can provide indirect evidence for halogen chemistry. Ozone destruction in tropospheric volcanic plumes, caused by volcanic halogen cycling, has been measured in a limited number of cases (Vance et al., 2010; Oppenheimer et al., 2010; Kelly et al., 2013; Surl et al., 2015). In ash-rich explosive eruptions, it is possible that uptake of ozone on ash particles may also contribute to some ozone loss (Maters et al., 2017). Measuring ozone in volcanic plumes in the troposphere region downwind from volcanoes is challenging and typically only achieved using instrumented aircraft. Another difficulty lies in attributing observed ozone losses to halogen chemistry when volcanic bromine emissions and/or bromine radical levels are not well-known. Observations suggest a direct relation between bromine content and ozone depletion (Roberts, 2018), although this is based on only three available volcanic datasets: Mount Etna, Mount Redoubt and Kilauea. Observations at Mount Redoubt volcano suggest that ozone losses, as a ratio to SO<sub>2</sub>, increase in magnitude with respect to the distance from the source (Kelly et al., 2013).

For the above methods, the observed halogen gas quantities or ozone depletions are often ratioed to simultaneous sulfur or SO<sub>2</sub> measurements. This allows for comparison between plumes of different "strengths" (i.e. density or dilution), and, for example, to trace how halogen chemistry changes as a plume disperses as it travels downwind. This use of SO<sub>2</sub> as a plume tracer presupposes that it has a long atmospheric lifetime relative to the timescale of the given study.

### 1.2.2 Numerical modelling

Another tool for studying the chemistry of volcanic plumes is numerical modelling. Most volcanic plume halogen chemistry modelling studies to date have originated from implementations of a few models, in particular MISTRA (Aiuppa et al., 2007;



Bobrowski et al., 2007; von Glasow, 2010; Bobrowski et al., 2015; Surl et al., 2015) and PlumeChem (Roberts et al., 2009,  
140 2014, 2018; Kelly et al., 2013). A more recent study by Rüdiger et al. (2020) used the CABBA/MECCA box model. These  
Lagrangian models are either zero- or one-dimensional and simulate the chemical evolution of the cooled plume by calculating  
the in-plume rates of chemical reactions and include the continual dilution of the plume with background air. Such models are  
found to better reproduce observations if the initial halogen emissions include a fraction of halogen radicals. This represents  
the radicals generated by high temperature chemistry in the effective source region.

145 To our best knowledge, Jourdain et al. (2016) is the only prior 3D Eulerian-type mesoscale chemistry-transport modelling  
study published to date dealing with halogen chemistry a tropospheric volcanic plume. Volcanic emissions and halogen chem-  
istry were implemented into the CCATT-BRAMS model to simulate the chemistry within the plume of Ambrym volcano  
during an intense passive degassing episode in 2005. Their model is similar to the one used in our study. However, their gas  
emission flux for the Ambrym event is about six times greater than the Mount Etna passive degassing event studied here.  
150 Mechanistically, their results showed the formation of BrO, as well as ozone depletion occurring within the plume's core that  
impacts bromine speciation. The study also simulated in-plume depletion of HO<sub>x</sub> and NO<sub>x</sub>, as well as lengthening of SO<sub>2</sub> and  
methane lifetimes due to halogen chemistry. The model successfully reproduced observed BrO/SO<sub>2</sub> spatial patterns, however  
the magnitude was somewhat underestimated, and there were no measurements of ozone to provide constraints on the predic-  
tions of ozone depletion, a key feature of reactive halogen chemistry. Finally, Jourdain et al. (2016) focuses on the wider-scale  
155 impact of volcanic emissions, whereas this study focuses more on the detailed mechanisms of halogen cycling in the early  
plume with cross-validation against ozone and halogen radical observations.

### 1.2.3 This study

The present study is devoted to a plume from Etna during July/August 2012, a period when this volcano was passively de-  
gassing. We present new airborne ozone and SO<sub>2</sub> measurements which were made during traverses of plumes at distances  
160 7–21 km from the vents. Several other previously published plume measurements were also made around this time. Near-  
simultaneous near-vent (<500 m) ozone measurements and DOAS observations of BrO/SO<sub>2</sub> ratios around 10 km downwind  
were reported by Surl et al. (2015). Additionally in situ sampling of halogen emissions was undertaken that summer at the  
crater-rim by Wittmer et al. (2014) and further DOAS measurements were also made of Etna's plume by Gliß et al. (2015).  
Consequently, this period of Etna's activity may have the richest overall dataset to date for determining halogen activity in  
165 relation to ozone loss in the plume of a volcano.

The observational dataset is analysed using a 3D regional chemistry-transport model (WRF-Chem) modified with respect to  
its handling of volcanic emissions and with halogen chemistry added to a chemical mechanism. The goal of the modelling is to  
assess the ability of the 3D model to adequately reproduce the key chemistry features (ozone loss, BrO/SO<sub>2</sub> ratios) of the Etna  
plume given reasonable input parameters, such as the typical halogen emission fluxes for the volcano in a passive degassing  
170 state. We then diagnose in-plume chemical processes in the model, exploiting the fact that a model can be interrogated in far  
greater detail than an observational dataset. The focus is on the chemical processes in the near-downwind plume, up to 10s of  
km from emissions sources for plume ages of up to 10s min. As well as halogen chemistry and the associated ozone destruction,



the simulated impacts of plume chemistry on the various interconnected chemical systems discussed above ( $\text{HO}_x$ ,  $\text{SO}_2$  lifetime and its oxidation to particles, methane lifetime, reactive nitrogen, and mercury chemistry) systems are also investigated.

## 175 2 Methods

### 2.1 Aircraft measurements of $\text{SO}_2$ and ozone in the plume

The aircraft campaign presented in this study was conducted as part of the Global Mercury Observation System project (<http://gmos.eu>) with the same aircraft and instrumentation discussed in Weigelt et al. (2016a) and Weigelt et al. (2016b). We refer the reader to these works for a full description of the campaign setup and instruments; in this section we highlight the most relevant aspects.

The measurements of this study were performed with a CASA 212 two-engine turboprop aircraft fitted with a specially designed gas inlet system.  $\text{SO}_2$  was measured with a Thermo Environmental Instruments Model 43C pulsed fluorescence gas analyzer with RMS noise of 1 ppbv and precision of 1 ppbv or 1% of reading ([http://www.thermo.com.cn/Resources/200802/productPDF\\_12267.pdf](http://www.thermo.com.cn/Resources/200802/productPDF_12267.pdf)). Estimates of the interferences from  $\text{H}_2\text{O}$  and  $\text{NO}$  are reported as  $< 3$  ppbv and  $< 2\%$  of reading. Ozone was measured with a Teledyne API 400E, with RMS noise and precision  $< 0.5\%$  of reading. This measurement is not subject to interference from  $\text{SO}_2$  or  $\text{H}_2\text{O}$  as these interferences are efficiently removed by the comparison of measurements between the ambient air channel and the ozone-scrubbed reference channel (<http://www.teledyne-api.com/products/oxygen-compound-instruments/t400>). Mercury vapour is listed as a potential source of interference; however mercury-detecting instruments were also active during this campaign and the level of gaseous mercury emission from the volcano was determined to be nil or low (Weigelt et al., 2016a). Both the  $\text{SO}_2$  and ozone instruments have a temporal resolution of 10s (averaging time) and their response times are 80 seconds and  $< 30$  seconds, respectively.

Three flights were conducted, one each on the mornings of 2012-07-30, 07-31, and 08-01, during daylight hours. These flights started and ended at Reggio Calabria Airport and attempted several transects of the plume. The flight paths are shown in Figure 2.

Since ambient concentrations of ozone vary both spatially and temporally, rather than assessing all of the observation data together, we undertook a systematic approach to identify and isolate separate "major plume encounters" from the dataset, and evaluate separately the ozone variations within these. This approach was designed such that the majority of the variation in ozone within each major plume encounter could be ascribed to plume chemistry rather than variations in the background. Our approach also fixed a maximum range of distances from the vent that could be considered part of a single major plume encounter so as to minimise any internal variation in ozone losses within a plume encounter due to plume chemistry varying with distance from the source. Ozone varies with altitude so we fixed a maximum range of altitudes that could be considered part of one major plume encounter — this avoids mistaking background ozone variation as the aircraft ascends or descends as a plume signal. Lastly, encounters that are too short or do not reach a sufficiently high plume intensity so as to allow for an identification of signal above background variation are dismissed.

Our algorithm is therefore as follows:

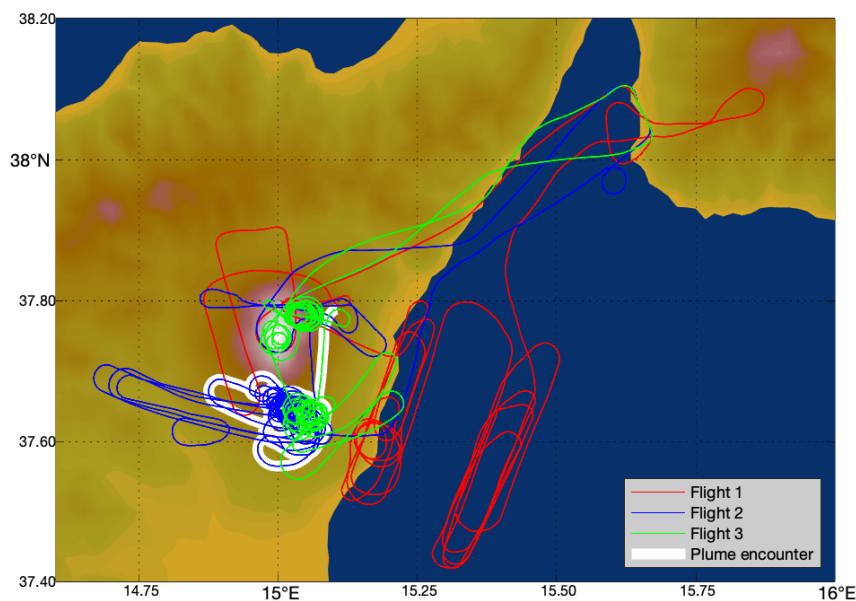


**Figure 2.** Flight paths of the aircraft on the three measurement days: red - 2012-07-30, blue - 2012-07-31, green - 2012-08-01. Major plume encounter locations as identified by our algorithm are highlighted in white.

- a plume encounter is considered to begin when the  $\text{SO}_2$  measurement exceeds 10 ppbv, and ends when  $\text{SO}_2$  drops below 10 ppbv
- If a datapoint's altitude is more than 300m higher or lower than that of any previous datapoint in the current encounter, the encounter ends and another immediately begins.
- 210 – If a datapoint's distance from the source is more than 5 km greater or smaller than that of any previous datapoint in the current encounter, the encounter ends and another immediately begins.
- if a plume encounter has maximum  $\text{SO}_2$  less than 100 ppbv, or lasts for less than 2 minutes, it is considered a "minor plume encounter" and is discarded

This process is presented in full as a flowchart in Figure S1.

## 215 2.2 Modelling

We use version 4.1.5 of WRF-Chem (Grell et al., 2005) which is a fully coupled three-dimensional regional model for atmospheric physics, meteorology and chemistry, including cloud and aerosol radiative feedback processes. We have made several





modifications to the code, in particular volcanic gas emissions and chlorine/bromine/mercury chemistry. We name this new model "WRF-Chem Volcano" (WCV). Our WCV developments build on the WRF-Chem version developed by the Roland von Glasow group at the University of East Anglia (Surl, 2016) and our WCV developments were made with reference to the model code of Badia et al. (2019), another development on the University of East Anglia version with a focus on marine chemistry.

### 2.2.1 Mechanism

WCV extends the CBMZ-MOSIAC chemistry scheme with 8 aerosol size bins (Zaveri and Peters, 1999; Zaveri et al., 2008) to include bromine, chlorine, and mercury chemical mechanisms with gas-phase, photolytic, and heterogeneous reactions involving the following species: HBr, Br, BrO, HOBr, BrNO<sub>3</sub> (a.k.a. BrONO<sub>2</sub>), Br<sub>2</sub>, HCl, Cl, ClO, OCIO, HOCl, ClNO<sub>3</sub>, Cl<sub>2</sub>, BrCl, Hg, HgBr, HgCl, HgBr<sub>2</sub>, HgCl<sub>2</sub>, and HgBrCl. We exclude BrNO<sub>2</sub> as previous studies have found it to be a negligible component (Roberts et al., 2014; Rüdiger et al., 2020). These species are also incorporated into the dry- and wet-deposition schemes and the FastJ photolysis scheme (Wild et al., 2000). The rates of heterogeneous reactions involving HOBr, BrNO<sub>3</sub>, and ClNO<sub>3</sub> on volcanic aerosols are calculated on-line accounting for the wet surface area of aerosol and gas-phase diffusion limitations as described by Marelle et al. (in review). The products of HOBr reactive uptake are partitioned between Br<sub>2</sub> and BrCl (i.e. net overall reaction with HBr or HCl) by a parameterization that assumes fast aqueous-phase equilibria between Br<sub>2</sub>, Br<sub>2</sub>Cl<sup>-</sup>, and BrCl as described by Jourdain et al. (2016). Reactions added to the scheme are listed in the supplement (Tables S1, S2, S4) along with their rate equations and references for these. Parameters controlling the heterogeneous reactions are tabulated in Table S3.

Our volcanic emissions pre-processor, a modified version of the the PREP-CHEM-SRC utility (Freitas et al., 2011), provides as inputs to the model fluxes of sulfur, bromine, chlorine, and mercury species as well as an 'at-source' sulfate particle flux, and fluxes of radicals resulting from high-temperature chemistry within the vent (e.g. OH, NO).

We have also introduced artificial tracer species to WCV that do not influence the chemistry but are useful for analysis. *tracer1* is a wholly inert species that is emitted with the same flux rate as SO<sub>2</sub>. *tracer1* is used to compute mean (weighted average) in-plume values of parameters — here an in-plume average of a value (e.g. of ozone mixing ratio) refers to the average of this value across all grid boxes where *tracer1* exceeds 3 ppbv, weighted by the *tracer1* content of the boxes.

*tracer2* is similar to *tracer1* but undergoes a first-order exponential decay with specified rate. The ratio of *tracer1* and *tracer2* can therefore be used to derive the mean time-since-emission of any part of the plume. This approach allows us to accurately calculate plume-age in any model grid cell and enables us to monitor how plume parameters (e.g. ozone mixing ratio, BrO/SO<sub>2</sub> ratio) vary with the plume time evolution since emission.

We have also added to the model output monitoring of several chemistry diagnostics, such as rates of relevant reactions, in order to carry out species' chemical budgets and therefore facilitate the analysis of the underlying halogen and ozone-destructive chemistry.



## 250 2.2.2 Model settings

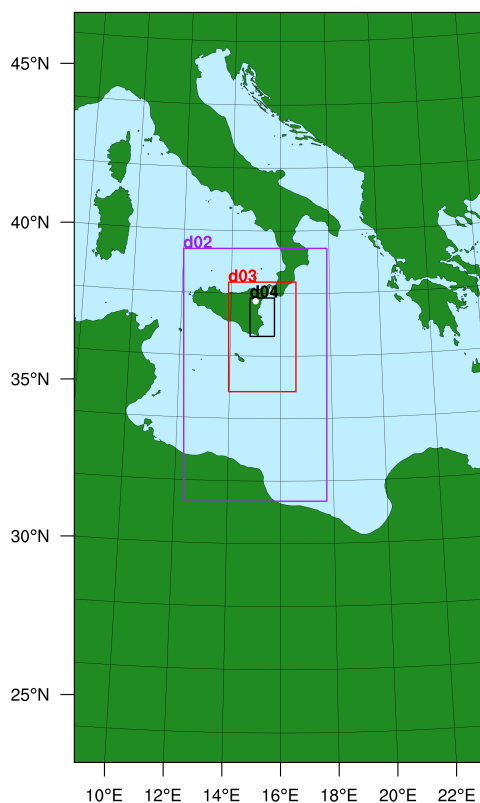


**Figure 3.** The WRF-Chem model area. *d02*, *d03*, and *d04* are progressively nested domains with two-way nesting.

The total area modelled, at 30 km horizontal resolution, is depicted in Figure 3. Also shown are the extents of the progressively nested domains, each modelled with grid dimension three times smaller than their parent. These domains are two-way nested in exchanging meteorological, chemical, and physical information between them. Here we focus on the near-downwind plume processing (up to about 90 minutes). Therefore all the figures and results presented in this study are from the *d04* nest  
255 which models an  $88 \text{ km} \times 134 \text{ km}$  area around the east coast of Sicily with a horizontal spatial resolution of 1.1 km. The model has 50 vertical layers, extending up to 50 hPa.

The model was initialised at 2012-07-29 00:00 and ran for four days, therefore covering all of the days of the aircraft measurements. The first 24 hours are considered spin-up, results are presented from > 24 hours onwards.

The volcano was considered to be a point source of gas and aerosol, emitting at a constant flux rate throughout the simulation  
260 period. Although Mount Etna has several active vents (North-east Crater, Voragine, South-East Crater) at the volcano summit, the maximum horizontal resolution of the model is not sufficient to distinguish these. Emissions are released into a single grid



cell at 37.751°N, 14.995°S, and 3300 mASL, the location of the summit peak of Etna. This altitude does not correspond to the lowest model level at this location but rather a few levels above it because, even at the maximum model resolution, the sub-grid topography of Etna volcano is smoothed out in the model grid box. For example, at the 1.1 km resolution, the ground altitude  
265 of the Etna grid box is 3088 m. The lower the model resolution is, the more potent the smoothing of sub-grid terrain features is, and hence the greater this discrepancy is.

Modelled emissions of SO<sub>2</sub> were set to 40 kg s<sup>-1</sup>. This flux was estimated by adjusting initial estimates according to comparisons between outputs from preliminary runs and observed SO<sub>2</sub> mixing ratios. A 40 kg s<sup>-1</sup> flux results in SO<sub>2</sub> mixing ratios within the centre of the modelled plume being similar to the maximum SO<sub>2</sub> mixing ratios observed from the aircraft  
270 at the same distance from the source. We assume these observed maxima correspond to transects which cross or comes close to the core of the plume. 40 kg s<sup>-1</sup> also falls mid-way within the normal range of measured SO<sub>2</sub> fluxes (41 ± 30) kg s<sup>-1</sup> for Etna's activity during non-eruptive (passive degassing) periods (Salerno et al., 2009). A volcanic H<sub>2</sub>O flux is set to be 15 times greater (in terms of number of molecules) than the SO<sub>2</sub> flux following Aiuppa et al. (2008). Being effectively inert chemically, CO<sub>2</sub> and its emissions are ignored in the model.

275 Mount Etna plume also contains sulfate-rich particles whose presence in the young plume at the volcano summit (Martin et al., 2012; Roberts et al., 2018) indicates they are formed early on, possibly in the vent, well below the grid resolution of the model. These 'at-source' aerosols are treated as primary aerosols. They are included in the model by setting a volcanic aerosol emission flux which is derived from the reported near-summit sulfate/SO<sub>2</sub> mass ratio of 0.03 (Roberts et al., 2018). All of this aerosol is taken to be sulfate with a size distribution into the 8 MOSAIC size bins following that of Roberts et al. (2018), with  
280 an extrapolation made for the smallest bins. Chlorine and bromine emission fluxes are specified based on the observed summit chlorine-to-bromine ratio and HCl-to-SO<sub>2</sub> ratio and the SO<sub>2</sub> flux specified above. We rely on a comprehensive compositional analysis undertaken between June 2010-June 2012 by Wittmer et al. (2014). The chlorine-to-bromine ratio was fixed to 300 by mass (683 by mole), which is an average calculated for the Bocca Nova and North-East craters' compositions reported by Wittmer et al. (2014). The HCl-to-SO<sub>2</sub> ratio was set to 0.4 mol/mol which is about mid-way in the range of ratios (0.29 to 0.56)  
285 for these craters.

As stated in the introduction, volcanic gases are believed to react at high temperatures immediately following their release in the vent and into the atmosphere, generating radicals, notably HO<sub>x</sub> and some halogen radicals. These radicals — as well as the primary aerosols — subsequently initiate the onset of the bromine cycling in the cooled plume (Figure 1). A representation of the high-temperature radicals is therefore needed for the WCV volcanic input. Thermodynamic models have been used previously to represent this high-temperature "effective source region" (Bobrowski et al., 2007) but their assumption of chemical  
290 equilibrium is not considered reliable, whereas recently developed kinetic models do not yet include halogens (see Roberts et al., 2019). Here we choose a simpler approach by partitioning the bromine emission flux into hydrogen halide and radicals, with 75% of bromine emitted as HBr and 25% as Br radicals, and by including a HO<sub>x</sub> emission. This bromine partitioning follows previous thermodynamic modeling estimates (Roberts et al., 2014). Emissions of volcanic HO<sub>x</sub> are highly uncertain,  
295 there exist order-of-magnitude differences between kinetic and thermodynamic model predictions, and in the speciation between OH and HO<sub>2</sub> (Roberts et al., 2019). Here, we define the volcanic HO<sub>x</sub> emission by setting a OH/SO<sub>2</sub> molar ratio of 0.001



(between reported thermodynamic and kinetic model ranges). The immediate reaction of OH with SO<sub>2</sub> in WCV will generate HO<sub>2</sub> and some additional sulfate. Whilst all volcanic chlorine is emitted as HCl in the model, the reaction with volcanic OH will also quickly generate some Cl radicals.

300 Although there are open questions regarding the kinetics of high-temperature NO generation in the first few seconds of plume evolution (Martin et al., 2012), we chose to include these emissions to assess its possible effect. We use an NO/SO<sub>2</sub> molar emission ratio of  $4.5 \times 10^{-4}$ , which is of the order typically produced by high temperature thermodynamic modelling of the early plume-air mix (c.f.  $6.6 \times 10^{-4}$  used in Roberts et al. (2014)).

305 Although the aircraft campaign did not find a detectable mercury signal for the plume (Weigelt et al., 2016a), we include a small mercury emission so as to investigate this mechanism. We use a general volcanic emission ratio of  $7.8 \times 10^{-6}$  mol Hg per mol SO<sub>2</sub> from Bagnato et al. (2014), a quantity too small to significantly interfere with other chemical systems. All of this mercury is emitted as Hg(0).

Species	Flux / s <sup>-1</sup>	Ratio to SO <sub>2</sub>	
		mass	molar
SO <sub>2</sub>	40 kg	1	1
Br	7.6 g	$1.89 \times 10^{-4}$	$1.5 \times 10^{-4}$
HBr	23 g	$5.66 \times 10^{-4}$	$4.5 \times 10^{-4}$
HCl	9.0 kg	0.226	0.4
OH	11 g	$2.7 \times 10^{-4}$	$1.0 \times 10^{-3}$
NO	8.4 g	$2.1 \times 10^{-4}$	$4.5 \times 10^{-4}$
H <sub>2</sub> O	169 kg	4.2	15
Hg	0.9 g	$2.4 \times 10^{-5}$	$7.8 \times 10^{-6}$
Aerosol	1.2 kg	0.03	0.02

**Table 1.** Volcanic emission fluxes in the *main* model run

We use external data for model forcing at the boundaries of the outermost domain and for the initial conditions of the model. Meteorological information is sourced from the NCEP FNL Operational Model Global Tropospheric Analyses (National Centers for Environmental Prediction et al., 2000). Chemical information is sourced from CAM-CHEM (Buchholz et al., 2019; Emmons et al., 2020) and applied using the MOZBC utility. Since mercury, bromine and chlorine species other than HCl were absent from this CAM-CHEM data, we set their initial and boundary values to zero.

315 As well as the main model run detailed above, several other model runs were made with varying emissions (Table 2). These include a model run with no volcanic emissions (*novolc*). Differences between *novolc* and the other runs are used to quantify volcanic impacts. Sensitivity runs were identical to the main run except for the perturbations to the volcanic emissions listed in Table 2. The *nohighT* run excludes all species expected to be generated in the high temperature volatile-air mix of the first few seconds after volcanic emission, and therefore includes only H<sub>2</sub>O, SO<sub>2</sub>, HCl, and HBr (all bromine as HBr) as well as primary sulfate.



Run name	Description
<i>main</i>	main model run
<i>novolc</i>	no volcanic emissions
<i>nohighT</i>	all bromine emissions as HBr, no OH or NO emissions
<i>mag33, mag150</i>	emissions of all species at 33%, and 150% of <i>main</i>
<i>hal00, hal33, hal150</i>	halogen emissions 0%, 33%, and 150% of <i>main</i>
<i>oth33, oth150</i>	emissions of all species except for HCl, HBr and Br at 33% and 150% of <i>main</i>

**Table 2.** Model runs in this study. Runs are identical to *main* with the exception of the perturbations to the modelled emissions listed

### 3 Aircraft observations quantifying ozone destruction in the plume

320 The encounter-finding algorithm described in Sect. 2.1 yields 19 major plume encounters, 11 on the 31st July and 8 on the 1st  
August 2012. Only minor plume encounters occurred on the 30th July. The locations of these major encounters are highlighted  
in Figure 2. Plots of O<sub>3</sub> vs. SO<sub>2</sub> for these encounters are shown in Figure 4 for the 31st July and Figure 5 for the 1st August.

For the majority of encounters, there is a clear anti-correlation between ozone and SO<sub>2</sub>, with linear fits yielding negative  
gradients. These observational data show that ozone is depleted within the plume, and this depletion is proportional to the  
325 intensity of the plume as quantified by SO<sub>2</sub> measurements.

Weighting by the duration of each encounter and their R<sup>2</sup> values, the average O<sub>3</sub> vs. SO<sub>2</sub> gradient for the plume encounters  
is -0.018 molec molec<sup>-1</sup>, and the average distance from the source is 14 km. Assuming that ozone destruction is a continuous  
process, and that, at distance zero, ozone destruction is zero, these value can be used to quantify the rate of ozone destruction  
as a ratio of SO<sub>2</sub> per km traveled; the resulting value is 0.0015 molec molec<sup>-1</sup> km<sup>-1</sup>. This could be converted to a destruction-  
330 per-second value by dividing by wind speed. No wind speed data was collected during the flights, so to do this we inspect the  
meteorological output from the model, which yields for both days a wind speed for the plume of approximately 9 m s<sup>-1</sup> at the  
time of the flights. Using this value yields a rate with respect to time of  $-1.3 \times 10^{-5}$  molec molec<sup>-1</sup> s<sup>-1</sup>. Interestingly, this  
rate is very close to a value of  $-1.0 \times 10^{-5}$  molec molec<sup>-1</sup> s<sup>-1</sup> derived from in-situ measurements made within 500 m of the  
vents on 27–30 July 2012 (Surl et al., 2015), supporting the theory of a continuous process beginning from no ozone depletion  
335 at source.

We note that an analysis to evaluate the trend in ozone depletion with respect to distance within the dataset yielded a null  
result: ozone depletion to SO<sub>2</sub> ratios were calculated for each in-encounter datapoint by using the y-axis intersect of each plume  
encounter as an estimate for background ozone for all datapoints within that encounter. The output from this analysis across  
the whole dataset was too noisy to discern an overall trend.

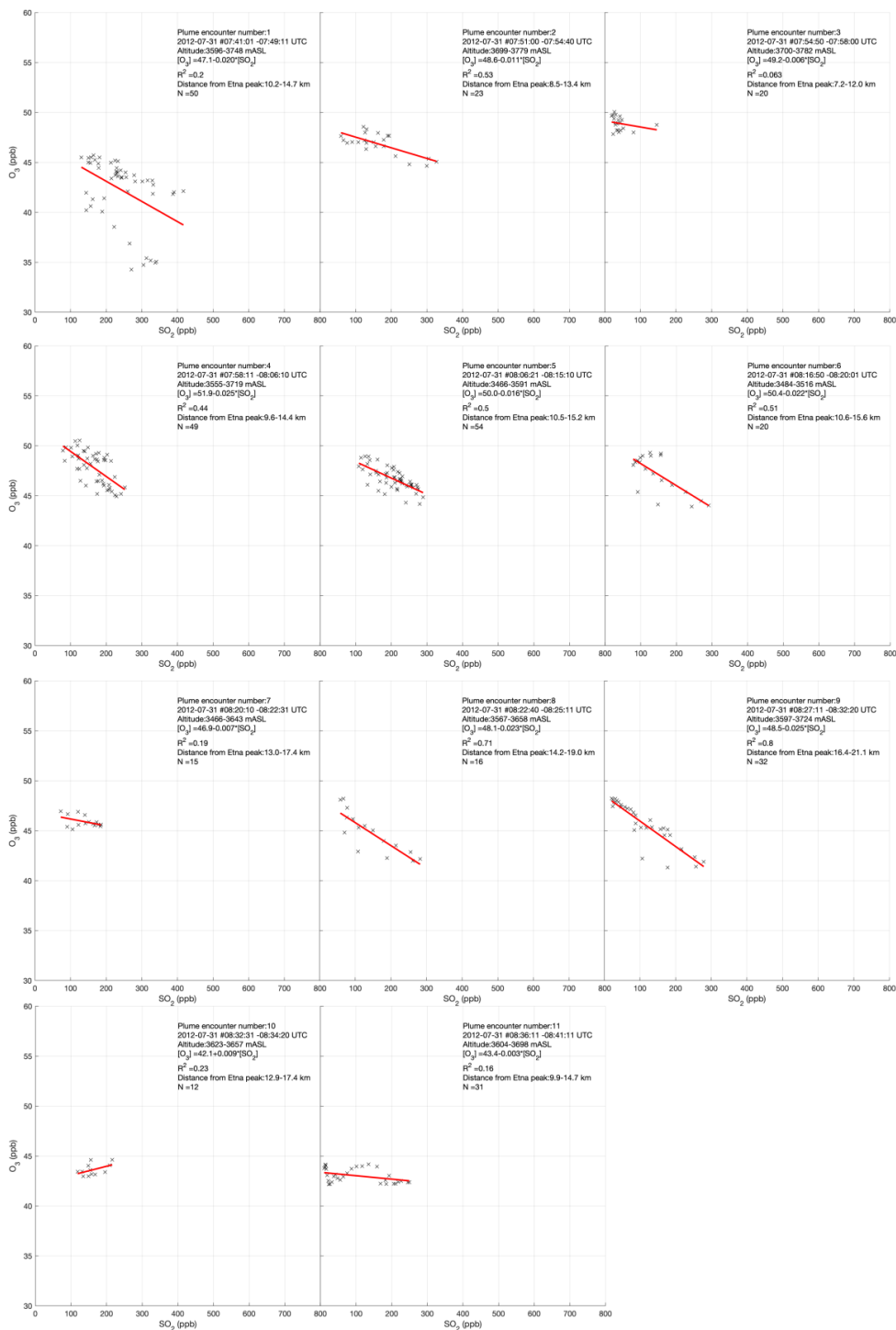
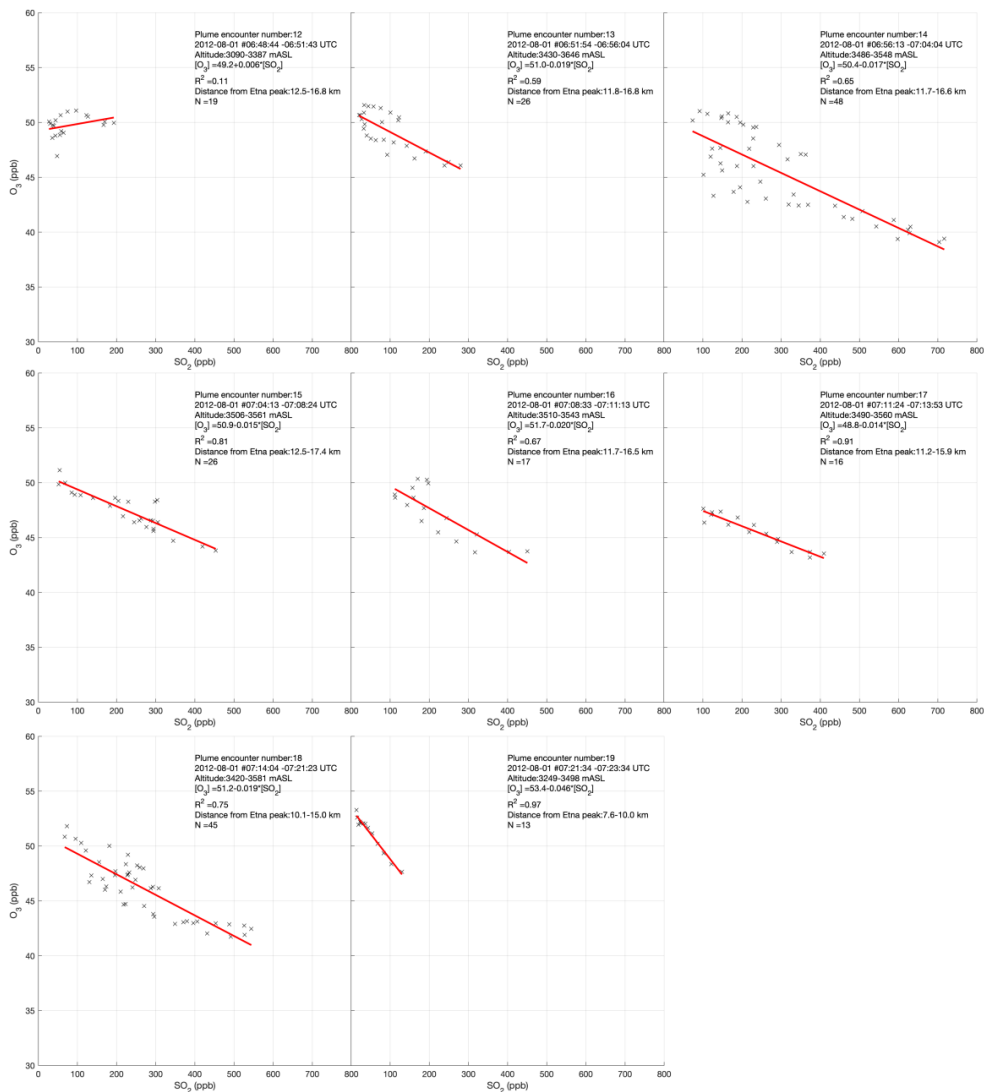


Figure 4. Measurements of  $\text{SO}_2$  and  $\text{O}_3$  mixing ratios for the 11 major plume encounters on 2012-07-31.



**Figure 5.** Measurements of SO<sub>2</sub> and O<sub>3</sub> mixing ratios for the 8 major plume encounters on 2012-08-01.



340 The observed depletion of ozone in Mount Etna plume is consistent with ozone-destructive halogen chemistry in volcanic  
plumes (Gutmann et al. (2018) and references therein). Halogens were not measured by the aircraft but ground-based remote  
sensing confirms the presence of volcanic BrO in the plume during July-August 2012 (Surl et al., 2015).

The following section presents the results of 3D high-resolution WCV model simulations, focusing on the ozone-destructive  
halogen chemistry in Mount Etna plume during the 2012 aircraft campaign. The model is used to quantify the ozone depletion  
345 and attribute it to specific halogen reactions, and to investigate additional impacts of volcanic plume halogen chemistry on  
atmospheric HO<sub>x</sub>, NO<sub>xy</sub> and mercury. Observational data and the model outputs are compared in Sect. 4.4.2, where parameters  
relating to the observed plume encounters and the linear regressions applied to them are also tabulated (Table 5) along with  
model data.

#### 4 Modelling of the atmospheric chemistry of Mount Etna's plume

350 All results discussed in this section are from the *main* model run unless otherwise stated. We have paid particular attention  
to the results relating to 0800 UTC on each of 2012-07-30, 07-31, and 2012-08-01 as the aircraft was sampling the plume at  
approximately this time.

In several cases we use plume age as a variable. This is determined from the tracers, as discussed in the Methods.

##### 4.1 SO<sub>2</sub>, aerosol, and HO<sub>x</sub>

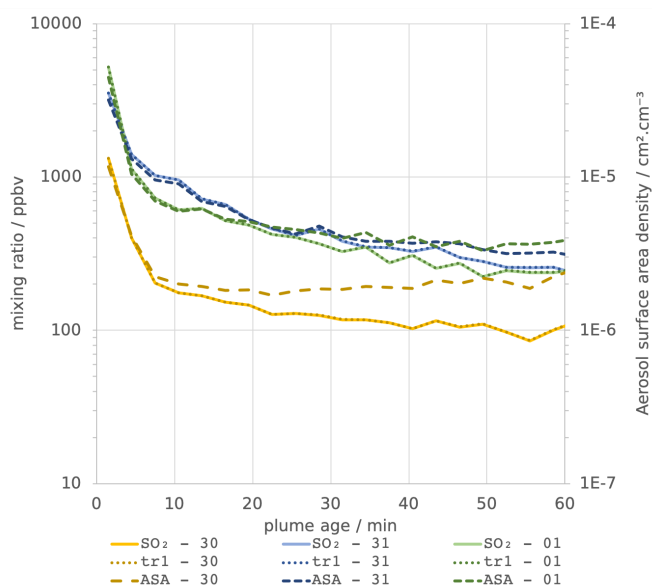


**Figure 6.** Modelled average in-plume mixing ratios of, on left axis, SO<sub>2</sub> (solid lines) and *tracer1* (tr1, dotted lines) and, on right axis, density of aerosol surface area (ASA, dashed lines). Note that both y-axes are logarithmic.





355 Before investigating the halogen chemistry of the volcano plume, we first look at  $\text{SO}_2$ . The volcano emits 40 kg of  $\text{SO}_2$  per second throughout the simulation. This produces a plume that travels downwind, dispersing (i.e. diluting) during transport –  $\text{SO}_2$  mixing ratios decrease with time and distance from the source (Figures 6, 14). The model  $\text{SO}_2$  chemistry includes gas-phase oxidation by OH, generating secondary sulfate aerosol.

For plumes aged less than an hour, the modelled mixing ratios of  $\text{SO}_2$  and *tracer1* in the plume are nearly identical (Figure 360 6), indicating that  $\text{SO}_2$  losses in this period are negligible. This gives confidence to the use of  $\text{SO}_2$  as a plume tracer, though we should note that the model does not contain other potentially significant  $\text{SO}_2$  loss mechanisms which occur in the liquid phase (Galeazzo et al., 2018).

Notably, the average mixing ratio of  $\text{SO}_2$  in the plume of the 30th July is significantly less than on the other two days, although the trend is similar. This difference is due to the fact that the wind speed on the 30th is much higher than on the other 365 two days: the average wind speeds in the < 60 min old plume at 0800 UTC are 19, 9, and 9  $\text{m s}^{-1}$  for the 30th July, 31st July, and 1st August respectively. Therefore, volcanic emissions are released into a greater volume of air on the 30th, yielding lower mixing ratios.

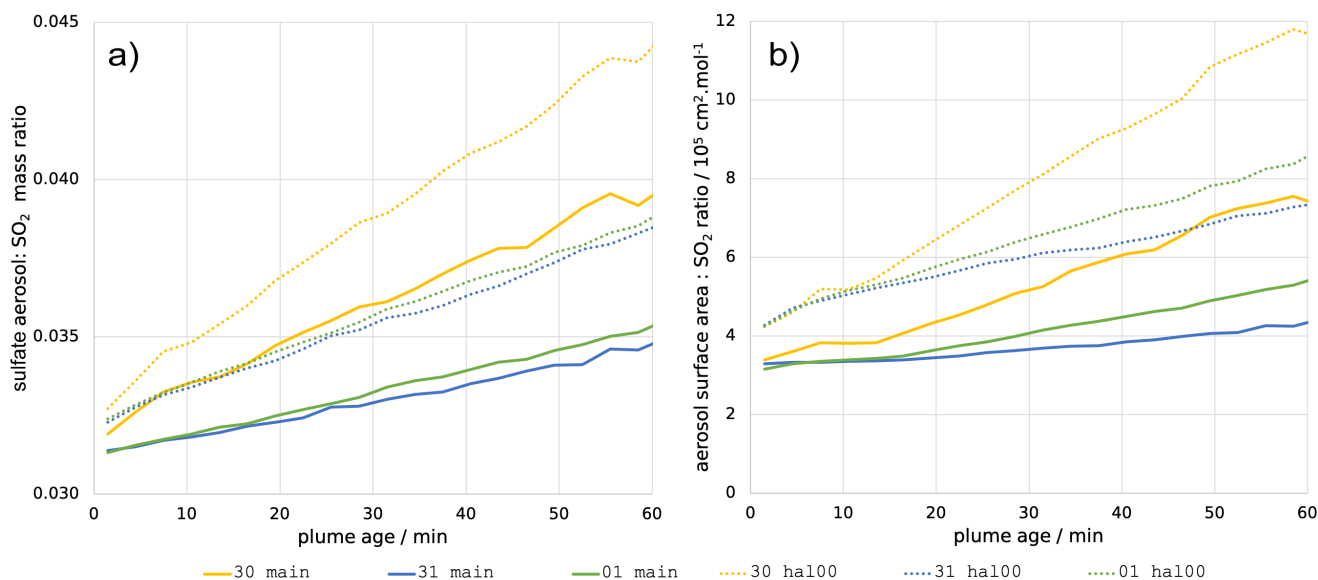


**Figure 7.** a) Mass ratio of sulfate aerosol to  $\text{SO}_2$  within the plume, and b) Ratio of the total in-plume aerosol surface area to  $\text{SO}_2$  concentration, both plotted against plume age for 0800 UTC for each of 2012-07-30 (yellow), 2012-07-31 (blue), and 2012-08-01 (green). Solid lines are for the *main* model run, dotted lines are for the *hal100* run.

The volcano is a direct source of aerosols, with a flux of 1.2 kg of sulfate per second in the model. This is important for the halogen chemistry as it provides a surface for HOBr uptake, enabling heterogeneous reactions. Figure 7a shows that, shortly 370 after emission, the in-plume ratio of sulfate to  $\text{SO}_2$  is slightly above the emission ratio of 0.03 because of the early oxidation of  $\text{SO}_2$  by volcanogenic OH (released in the emission grid box to account for high-temperature radical production) which



produces additional sulfate. This ratio continues to increase with plume age due to ambient temperature oxidation by OH mixing in from background air.

There are similar trends for the aerosol surface area-to-SO<sub>2</sub> ratio (Figure 7b), the increase in this ratio shows that the secondary aerosol formation notably increases the surface area available for HOBr uptake. When considered in absolute terms, this secondary aerosol formation partly offsets the decline in aerosol surface area density caused by plume dispersion. This can be seen on Figure 6 where the aerosol surface area density declines at a slower rate than SO<sub>2</sub> mixing ratio. For the 30th the aerosol surface area density is approximately constant after 10 minutes, indicating that the secondary formation compensates for the dispersion in this regard.

Although the oxidation of SO<sub>2</sub> is not significant over these time scales with regard to SO<sub>2</sub> mixing ratios, the oxidation that does occur is significant for in-plume aerosol and HO<sub>x</sub> levels. There is a substantial depletion of OH within the plume, and a

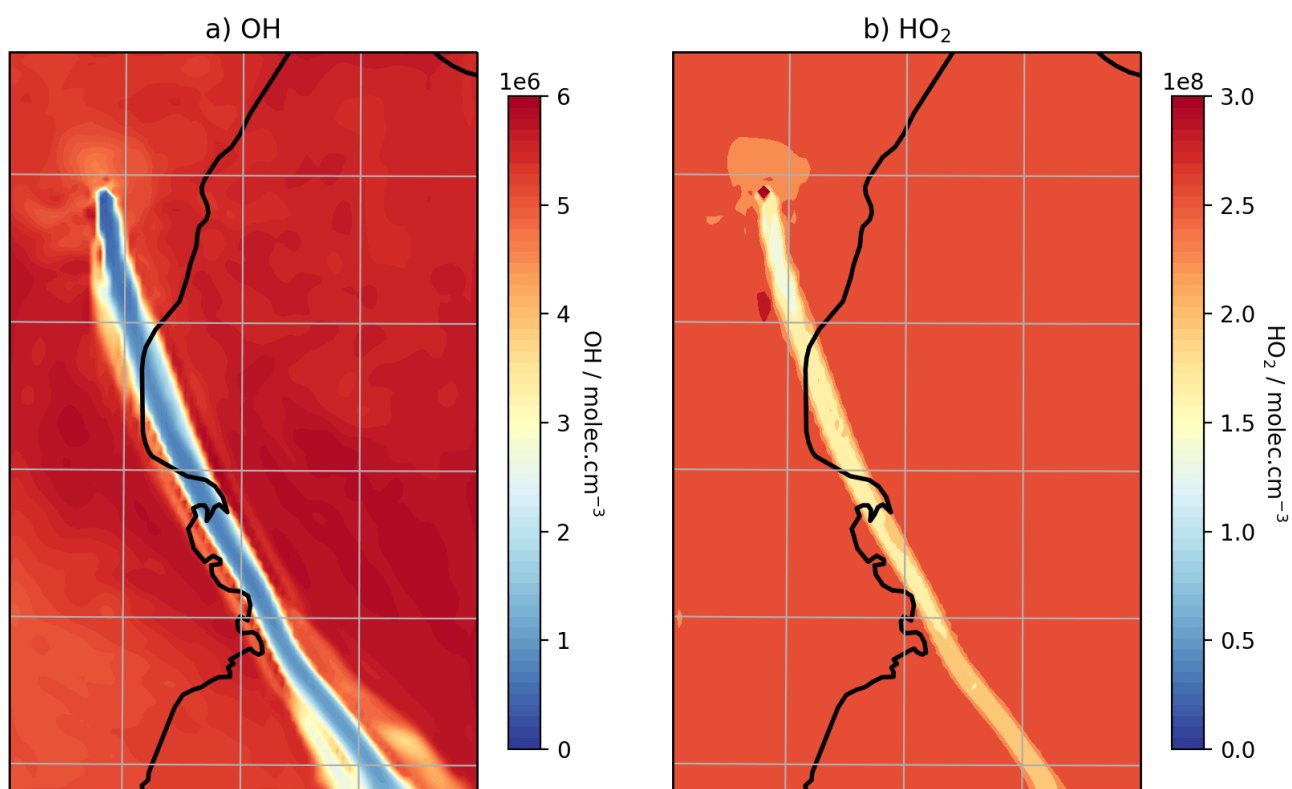


**Figure 8.** Modelled mixing ratios of a) OH and b) HO<sub>2</sub> at 3300mASL at 0800 UTC on 2012-08-01.

moderate depletion of HO<sub>2</sub> (Figure 8). This result is consistent with model findings for the Ambrym plume (Jourdain et al., 2016), and occurs despite the modelled volcano being a source of OH — this emitted OH is consumed very quickly.

Volcanic halogens and SO<sub>2</sub> compete for reaction with the available OH. The abundance of SO<sub>2</sub> in the plume results in substantial conversion of OH to HO<sub>2</sub> via the SO<sub>2</sub> + OH reaction. This starts a chain of reactions with short-lived intermediate



model run	HO <sub>2</sub> / molec cm <sup>-3</sup>	OH / molec cm <sup>-3</sup>	SO <sub>2</sub> lifetime / h
<i>novolc</i>	2.6 × 10 <sup>8</sup>	5.8 × 10 <sup>6</sup>	53
<i>hal00</i>	4.6 × 10 <sup>8</sup>	1.4 × 10 <sup>6</sup>	240
<i>main</i>	1.6 × 10 <sup>8</sup>	0.9 × 10 <sup>6</sup>	390

**Table 3.** In-plume concentrations of HO<sub>2</sub> and OH and instantaneous lifetime of SO<sub>2</sub> with respect to oxidation by OH for plume aged 30 ± 5 min at 0800 UTC on 2012-08-01 for three model runs. Figures for the *novolc* use the same grid cell weighting as the *main* model run.

species that simplified to a single SO<sub>2</sub> + OH → HO<sub>2</sub> + H<sub>2</sub>SO<sub>4</sub> reaction in the model (Bekki, 1995; Galeazzo et al., 2018). Volcanic HCl is also abundant and removes OH by the HCl + OH → H<sub>2</sub>O + Cl reaction. A similar reaction of HBr also occurs, but HBr is much less abundant. HO<sub>2</sub> is consumed as part of the bromine cycle in the BrO + HO<sub>2</sub> → HOBr reaction.

Table 3 compares the weighted average mixing ratios of HO<sub>x</sub> species and the instantaneous SO<sub>2</sub> lifetime within the plume for the *main* run, the halogen-free *hal00* run, and the equivalent model cells in the plume-free *novolc* run. Comparing these, it can be seen that the non-halogen components of the plume are sufficient to cause substantial OH depletion, whilst halogens are the cause of HO<sub>2</sub> depletion — the *hal00* plume actually has greater HO<sub>2</sub> compared to the *novolc* case.

Although the instantaneous lifetime of SO<sub>2</sub> (with respect to oxidation by OH) is substantially increased in the halogen-free model plume, we note that the addition of halogen emissions to the model further suppresses OH, increasing the SO<sub>2</sub> lifetime and having a reductive effect on secondary aerosol production both in terms of mass and surface area (Figure 7). This result for a tropospheric volcanic plume mirrors findings from a recent study of a stratospheric volcanic cloud (Lurton et al., 2018).

Whilst a detailed analysis of the aerosol microphysics and climate impacts of volcanic aerosols lies beyond the scope of this study, our simulations show substantial differences in the plume sulfate particle surface area density for WCV model simulations with and without volcanic halogen emissions. As plume halogen chemistry exerts an important influence on the oxidation rate of volcanic SO<sub>2</sub> and associated formation of secondary aerosol, our results suggest that models simulating chemistry-climate impacts of volcanic sulfur should not ignore the chemistry of volcanic halogens.

## 4.2 Bromine speciation and BrO/SO<sub>2</sub> ratio

In the model output, the bromine is emitted from the volcano as HBr and Br in a 3:1 ratio. During daylight this is rapidly converted to other forms, including BrO. Figure 9 shows how the forms which this bromine takes vary between plume of different ages at 08:00 UTC on the 30th, 31st and 1st. In this model output, HOBr becomes the dominant form of bromine within the plume, followed by BrO. The fraction as BrO increases over approximately the first 20 minutes before reaching an approximately stable fraction. A significant amount of Br<sub>2</sub> is formed shortly after emission but this fraction declines, with BrCl being the larger fraction of the two halogen dimers. A significant reservoir of BrNO<sub>3</sub> that forms shortly after emission declines slowly over time.

There are significant quantitative differences between the bromine evolution on these three days, although the trends are similar. These differences occur despite the emission parameters being the same for all days. Compared to the other two days,

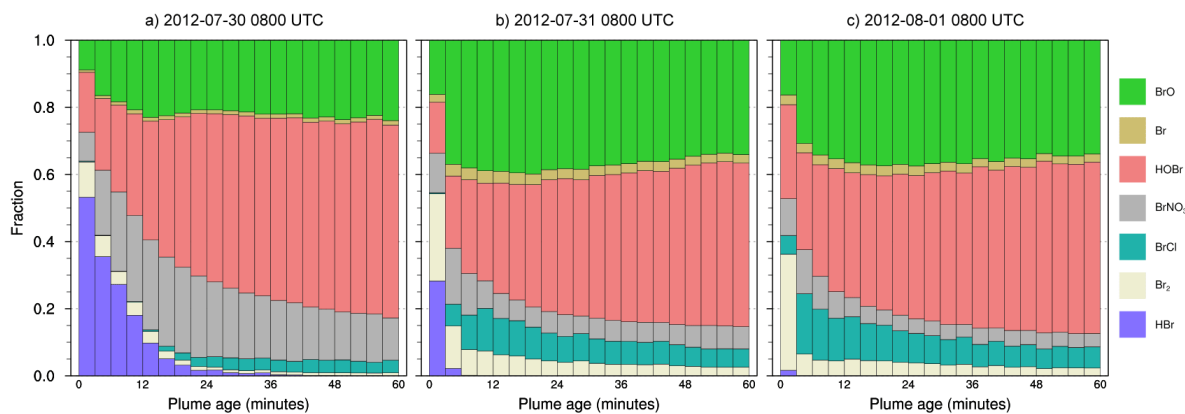


**Figure 9.** Differentiation of bromine between species for plume of different ages ranging from 0–60 minutes, for plume at 08:00 UTC on a) 2012-07-30, a) 2012-07-31, c) 2012-08-01

HBr and  $\text{BrNO}_3$ , and HOBr persist in the plume for much longer, on the 30th July. The balance between HOBr and BrO is more greatly tilted towards the former on that day because the in-plume aerosol surface area density is lower on the 30th, reducing the rate of heterogeneous reactions that consume HBr,  $\text{BrNO}_3$ , and HOBr. Additionally, the reaction of BrO with background  
415  $\text{HO}_2$  to form HOBr is suppressed under more concentrated plume conditions due to the depletion of  $\text{HO}_2$  discussed in Sect. 4.1.

Although the bromine speciation appears roughly stable after approximately 30 minutes of evolution, this does not indicate that no further chemistry is occurring, bromine is continually cycled between forms. This is shown in Figure 10 which depicts the rates of transfers between bromine species. "Stability" indicates a state where the chemical formation and loss of each  
420 species is approximately balanced, i.e. a steady state.

The ratio of total bromine and  $\text{SO}_2$  is mostly invariant in the plume, therefore the variations in bromine speciation with plume age yield variations of in-plume  $\text{BrO}/\text{SO}_2$  ratios. There is an initial rise in  $\text{BrO}/\text{SO}_2$ , followed by a small decrease in some cases, and then a plateau. This pattern varies with time of day, as shown in Figure 11. Sunrise is shortly after 04 UTC and sunset shortly after 18 UTC. Negligible BrO is formed in the model plume at night. We find on all three days that  $\text{BrO}/\text{SO}_2$  ratios  
425 are generally greater in the morning and evening than during the middle of the day. This occurs because BrO is more rapidly converted to HOBr in the middle of the day when atmospheric  $\text{HO}_2$  is at a maximum. Although moderate in magnitude, this phenomenon may be significant when comparing spectroscopic columns at different times, including datasets from low-earth orbit satellites with overpasses at different local times.

Our model study identifies how variations in time-of-day and plume intensity (which is controlled by wind speed in this  
430 constant-emission case) impact  $\text{BrO}/\text{SO}_2$ . These may present additional complications for the interpretation of  $\text{BrO}/\text{SO}_2$  ratios observed in passively degassing volcanic plumes. Variations of  $\text{BrO}/\text{SO}_2$  are often evaluated with respect to distance from a volcano. We note that the wind speed has a "double effect". First, faster winds give the impression that the chemistry evolves

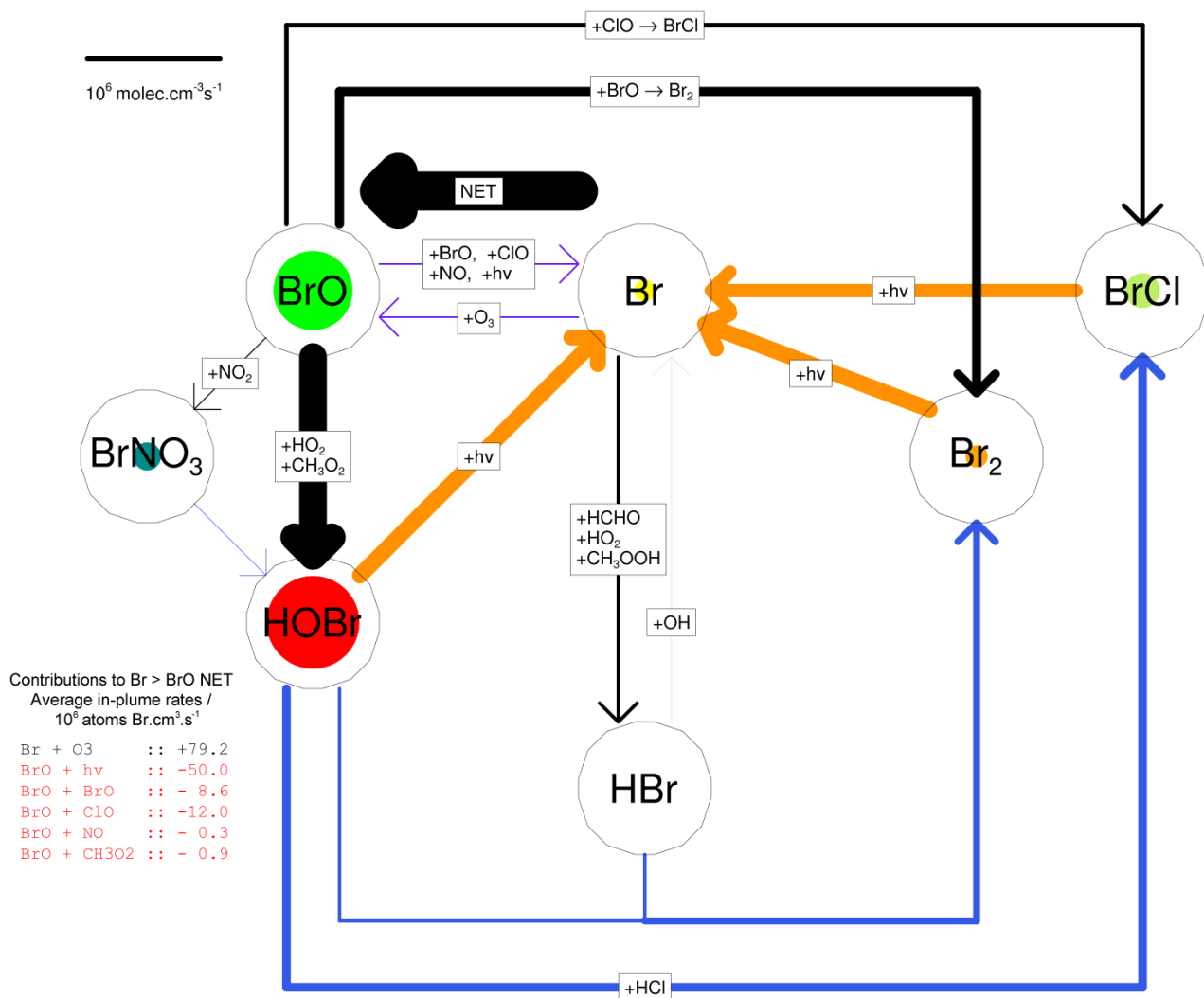


**Figure 10.** The in-plume bromine cycle in the plume for plume aged 30-60 minutes at 2012-08-01 0800. Areas of the coloured circles are proportional to the fraction of total bromine present as that species, a fully coloured circle would correspond to 100%. Widths of lines are proportional to the weighted average rate of these reactions in the plume, see reference line top left for scale. Orange lines indicate photolysis reactions, blue lines heterogeneous reactions, black lines other gas-phase reactions. The rates of reactions contributing to the Br  $\rightleftharpoons$  BrO interchange are depicted bottom left, only the net Br  $\rightarrow$  BrO flux is shown.

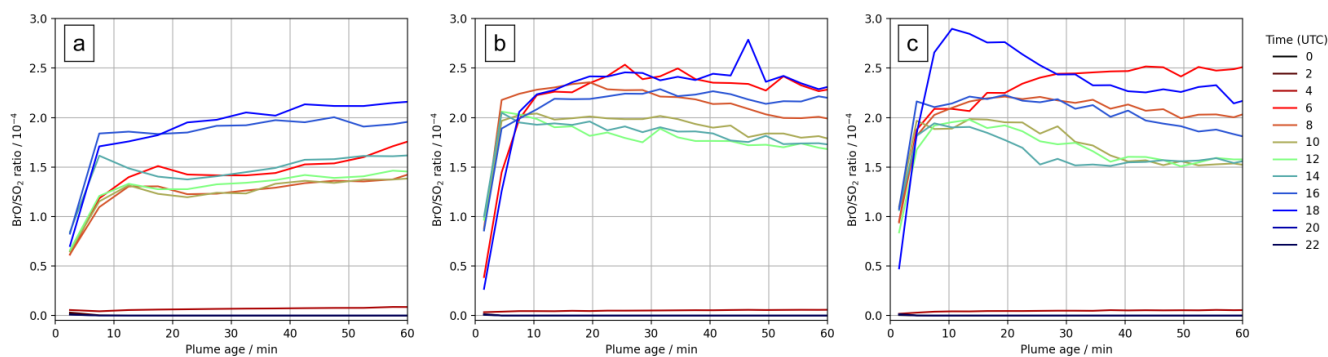


**Figure 11.** In-plume average BrO/SO<sub>2</sub> ratios for plume of different ages ranging from 0–60 minutes, at several times on a) 2012-07-30, b) 2012-07-31, c) 2012-08-01

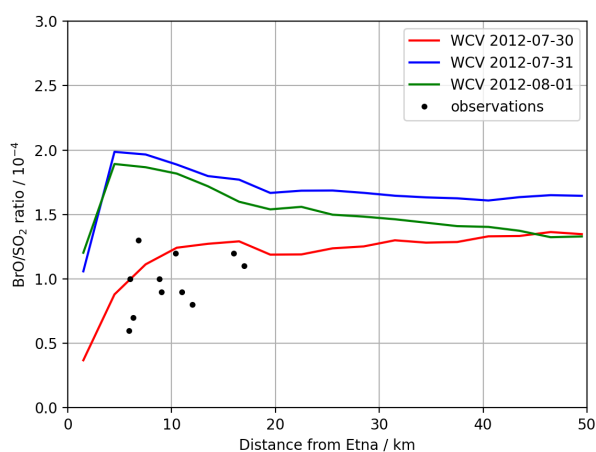


**Figure 12.** Modelled BrO/SO<sub>2</sub> ratio at 1200 UTC on 2012-07-30, 2012-07-31, and 2012-07-31 (lines), and observed BrO/SO<sub>2</sub> ratios for 2012-07-24 – 2012-08-02 (Surl et al., 2015) (circles), plotted against distance from the volcano. We caution that these observations, taken over several days with varying wind speeds, should not be interpreted as representing temporal evolution.



more slowly as a function of distance downwind because the plume moves further from the source in a given time. Second, all other factors being equal, the along-plume dilution is expected to be stronger at higher wind velocities, affecting the in-plume chemistry and bromine speciation through the influx of background ozone-rich air.

#### 4.2.1 Comparison to observed BrO/SO<sub>2</sub> ratios

No measurements of in-plume BrO/SO<sub>2</sub> column ratio were made as part of this study. However the DOAS-measured BrO/SO<sub>2</sub> columns reported in Surl et al. (2015) span from 2012-07-24 to 2012-08-02 which includes our time period. These observations were made between 5 and 17 km from the volcano at approximately the middle of the day. Figure 12 plots these observations alongside the modelling data for 12 UTC each day. These observed ratios, ranging from  $0.6 - 1.3 \times 10^{-4}$ , are at about half of the equivalent modelled ratios for the 31st July and the 1st August, and are comparable, although still slightly lower on average, to those modelled for the 30th, where the initial rise in BrO/SO<sub>2</sub> ratios occurs over the first 15-20 km.

Although not simultaneous with the time span of this study, BrO/SO<sub>2</sub> measurements made close to the vents the following month (2012-09-11 – 2012-09-26) reported by Gliß et al. (2015) are also a relevant comparison. BrO/SO<sub>2</sub> ratios were found rising rapidly with travel time from the vent, reaching about  $1.3 \times 10^{-4}$  at about 150 seconds travel time and then remaining at this level. This rapid rise, and higher ratio, has better agreement with the observations of the 31st and 1st.

More generally, the shape of the modelled BrO/SO<sub>2</sub> versus distance/time trend seen in Figures 11, 12, and 13a — of an initial rise followed by a steady value — is in agreement with the general trend observed for Etna and other volcanoes (Gutmann et al., 2018).

#### 4.2.2 Importance of high-temperature volcanic products

The modelled conversion of HBr into BrO and other forms is much slower in the *noHighT* run (Figure S2). This indicates the importance of initial volcanogenic radicals from the “effective source region” in the autocatalytic processes of the bromine explosion. In their absence this process is nonetheless initiated, but it is only partially completed even for 60 minutes plume age. Note however that the model does not have any background bromine, which in the absence of volcanogenic radicals could potentially contribute to initiating this process.

### 4.3 Chlorine species

The uptake to particles and subsequent reaction of HOBr with hydrogen halides (HBr, HCl) has the effect of transferring halogen from halides to reactive forms. When HBr and HCl are both present in the plume the product of this is almost exclusively Br<sub>2</sub>. However after a short time HBr is almost totally depleted in the plume and is consumed as fast as it is produced, whereas HCl remains abundant. The subsequent photolysis of BrCl produces reactive chlorine. This reactive chlorine forms the spectroscopically detectable species ClO and OClO within the plume — the reaction of Cl with ozone produces ClO, and the reaction of ClO with BrO produces OClO. Figure 13 shows the vertical columns of these species within the plume as ratios

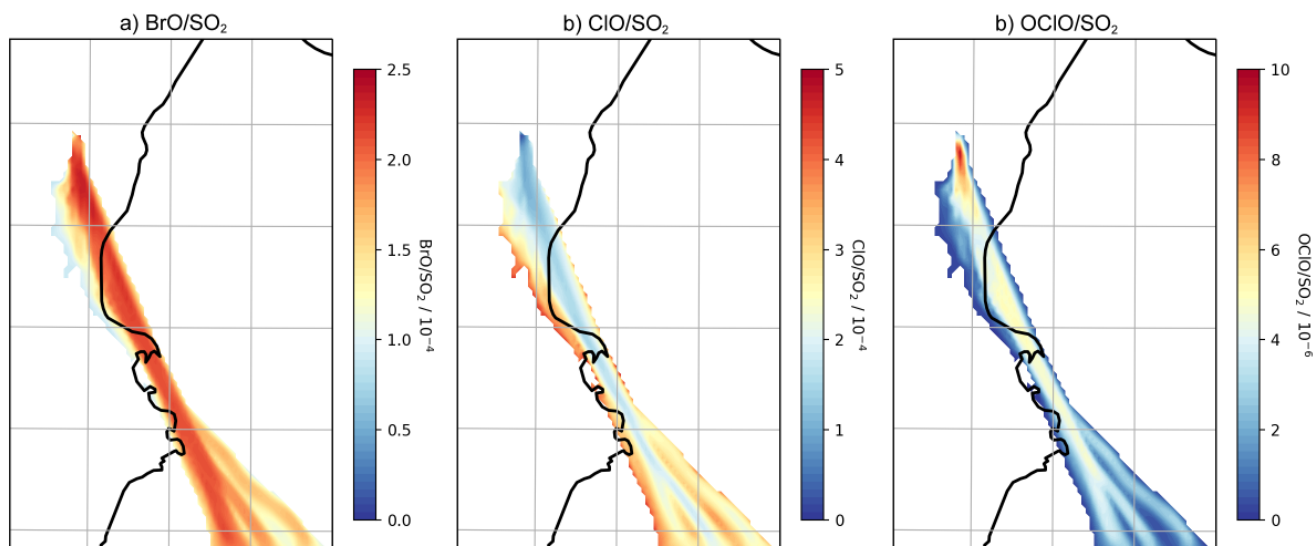


**Figure 13.** Model column ratios at 0800 UTC on 2012-08-01: a) BrO/SO<sub>2</sub>, b) ClO/SO<sub>2</sub> c) OCIO/SO<sub>2</sub>. Only columns with a modelled SO<sub>2</sub> density greater than  $2 \times 10^{16}$  are plotted.

of the SO<sub>2</sub> column. ClO/SO<sub>2</sub> ratios are of similar magnitudes (a few  $10^{-4}$ ) to BrO/SO<sub>2</sub>. OCIO/SO<sub>2</sub> ratios are about two orders of magnitude lower, except for very close to the emission point where they approach  $1 \times 10^{-5}$ .

465 Spatially, lower ClO/SO<sub>2</sub> column ratios are found in the more concentrated parts of the plume (and higher ClO/SO<sub>2</sub> at the plume edges). Conversely, OCIO/SO<sub>2</sub> shows the opposite spatial pattern, and is highest shortly after emission, because of the initial burst in OCIO production from ClO and BrO in the concentrated early plume.

OCIO and ClO are rarely observed above instrumental detection limits in volcanic plumes. Our model results are broadly consistent in magnitude with the few reported OCIO observations in in Etna plume reaching  $1 \times 10^{-5}$  (Gliß et al., 2015) whilst  
470 General et al. (2014) report OCIO/SO<sub>2</sub> up to  $10^{-4}$  mol/mol. Some observational studies (Bobrowski et al., 2007; General et al., 2014) report greater BrO/SO<sub>2</sub> and OCIO/SO<sub>2</sub> at the plume edges compared to the centre, which is not seen in our model. This might be due to the horizontal spatial resolution of WCV, or it might reflect a real difference in the chemistry of the plume. Note that box-modeling findings indicate that the magnitude of such ‘edge effects’ depends on volcanic conditions such as emitted the HBr/SO<sub>2</sub> (Roberts et al., 2018).

475 High levels of CH<sub>4</sub>-oxidising chlorine radicals (Cl) in the plume reduce the instantaneous lifetime of CH<sub>4</sub> in the plume, which, in the early plume considered here, more than compensates for the decrease in CH<sub>4</sub> oxidation from the reduced levels of OH. However, at the edges of the plume, the lifetime-extending effect is greater, leading to the spatial pattern seen in Figure S4. Oxidation of CH<sub>4</sub> produces HCHO, and therefore the plume has elevated mixing ratios of this species (Figure S5).



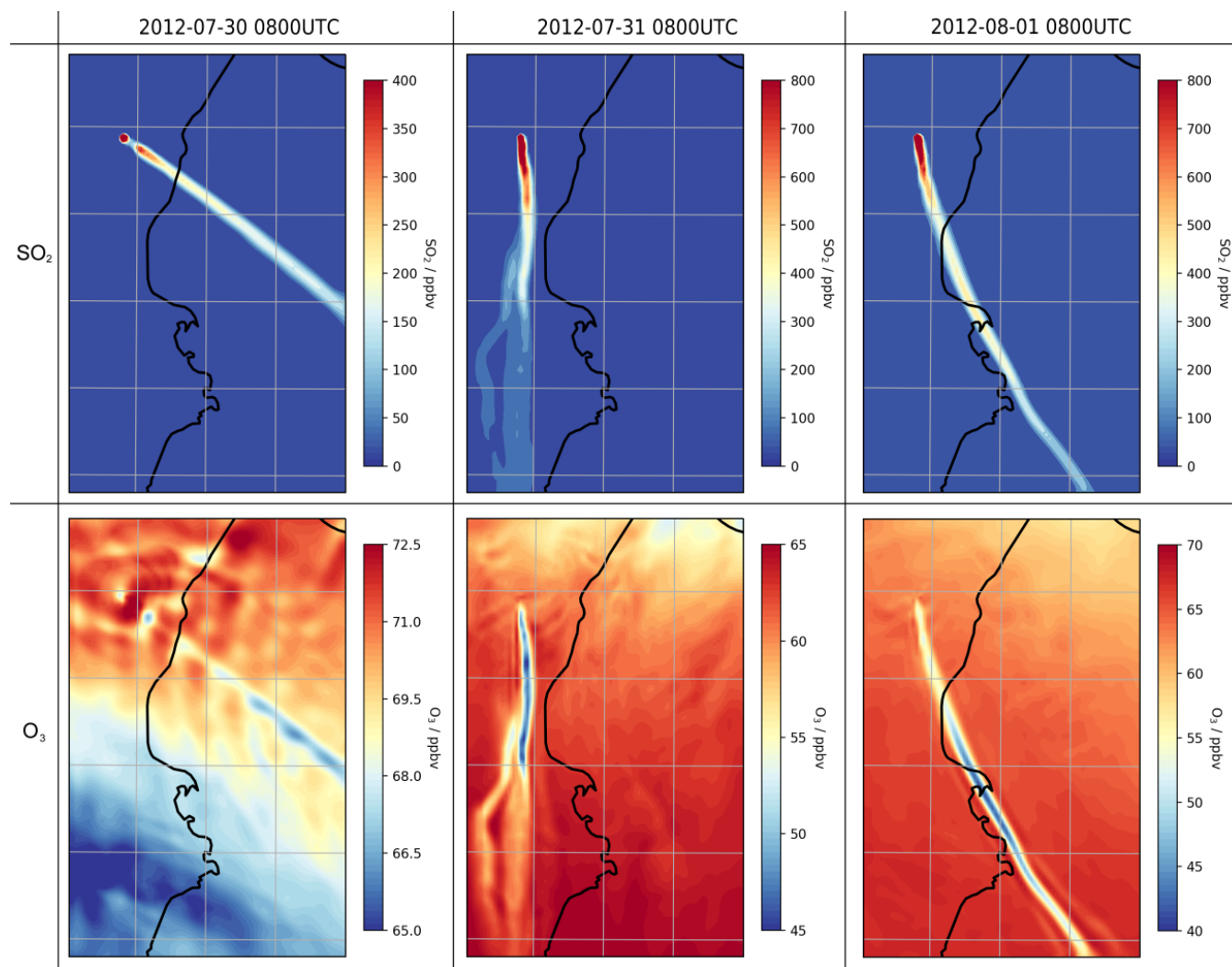


**Figure 14.** Modelled mixing ratios of SO<sub>2</sub> (first row) and O<sub>3</sub> (second row) at 3300mASL (volcano height) in the model at 0800 UTC on 2012-07-30 (first column), 2012-07-31 (second column), and 2012-08-01 (third column). Different colour scales are used for each subplot



#### 4.4 Ozone depletion

480 During the day, ozone levels are lower in the plume than in the surrounding air (Figure 14). On the 30th, the in-plume ozone loss is only a few ppbv, whereas it reaches of the order of a few 10s of ppbv on the 31st and 1st.

Comparing output from the *main* and *novolc* model runs allows for a precise calculation of  $\Delta O_3$ , the change in ozone due to the volcano. Following the approach used in Kelly et al. (2013) and Surl et al. (2015), we compute  $\Delta O_3/SO_2$  to isolate the chemical signal from physical dispersion effects. Figure 15 shows the variation of this ratio with plume age at different  
485 times of day. Because this ozone destruction is slower on the 30th compared to the other two days, and because the plume is travelling faster due to the greater wind speed, the smaller ozone loss on 30th compared to the other days is even more apparent if  $\Delta O_3/SO_2$  is plotted against distance (Figure 16). The absence of halogen chemistry means that, at night,  $\Delta O_3/SO_2$  is close

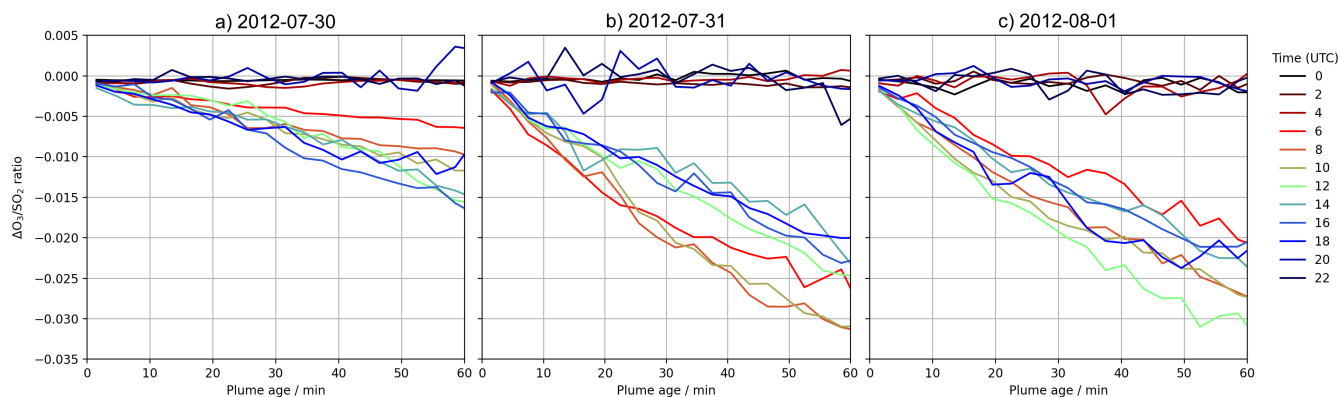


**Figure 15.** In-plume average  $\Delta O_3/SO_2$  ratios for plume of different ages ranging from 0–60 minutes, at several times on a) 2012-07-30, b) 2012-07-31, and c) 2012-08-01. Only ratios where the corresponding  $SO_2$  column exceeds  $2.0 \times 10^{16}$  molec  $cm^{-2}$  are shown.

to zero. During the day the ratio is negative, and increases in magnitude with plume age. This indicates that chemical ozone destruction in the plume is a continuous, ongoing, process. Although the data depicted in Figure 15 are Eulerian snapshots  
490 rather than Lagrangian traces of the plume, these lines' gradients are an indication of the rate of the ozone loss process. For 2012-08-01 08:00, the gradient is about  $-7.5 \times 10^{-6}$  molecules of  $O_3$  per molecule  $SO_2$  per second.

Secondly, by inspecting the rates of reaction for the *main* model run as shown in Figure 10, and computing the differences between the rates of ozone-destructive and ozone-forming reactions, we find that these halogen reactions result in an average net ozone loss rate of  $3.1 \times 10^7$  molec  $cm^{-3} s^{-1}$  within this part of plume. Dividing this by the weighted average plume  $SO_2$   
495 mixing ratio yields an instantaneous loss rate of of  $7.1 \times 10^{-6}$  molecules of  $O_3$  per molecule  $SO_2$  per second, very close to the value determined by the prior method.



Reaction	Fraction at plume age...			
	15min	30min	45min	90min
$\text{BrO} + \text{BrO} \rightarrow 2 \text{Br} \text{ or } \text{Br}_2 + \text{O}_2$	44%	40%	34%	28%
$\text{BrO} + \text{ClO} \rightarrow \text{Br} + \text{Cl} \text{ or } \text{BrCl} + \text{O}_2$	21%	21%	22%	22%
$\text{BrO} + \text{ClO} \rightarrow \text{OClO} + \text{Br}$	21%	21%	21%	25%
$\text{BrO} + \text{NO} \rightarrow \text{Br} + \text{NO}_2$	1%	1%	1%	1%
$\text{BrO} + \text{CH}_3\text{O}_2 \rightarrow \text{Br} + \text{HCHO} + \text{HO}_2$	1%	2%	3%	4%
$\text{HOBr} \xrightarrow{h\nu} \text{Br} + \text{OH}$	5%	8%	11%	13%
$\text{HOBr} + \text{HBr} \xrightarrow{\text{het}} \text{Br}_2 + \text{H}_2\text{O}$	2%	2%	2%	3%
$\text{HOBr} + \text{HCl} \xrightarrow{\text{het}} \text{BrCl} + \text{H}_2\text{O}$	6%	4%	6%	6%

**Table 4.** Modelled relative fractions of bromine reduction by the various non-O<sub>3</sub> forming reactions for plume of difference ages ( $\pm 5$  mins listed age) at 2012-08-01 08:00

#### 4.4.1 Attribution of ozone loss to halogen reactions

A detailed analysis of the model outputs allows us to attribute ozone loss to specific bromine reaction cycles. Ozone is destroyed by its reaction with Br to form BrO, but the net ozone loss depends on the subsequent fates of BrO and HOBr (the product of BrO and HO<sub>2</sub>). If BrO undergoes a reduction chemistry that reforms ozone there is no net impact, while if a reduction path does not reform ozone there is a net ozone loss. Table 4 tabulates the relative rates of the BrO and HOBr reduction reactions which yield Br, Br<sub>2</sub>, or BrCl without reforming ozone in the plume and therefore can be "credited" with ozone destruction. We find that for this young plume, the most important of these bromine reduction reactions are the reactions of BrO with itself and of BrO with ClO, which together account for about three-quarters of the bromine recycling.

The relative importance of the BrO self-reaction decreases slightly as the plume dissipates and evolves, whilst the two reactions of BrO with ClO maintain the approximately same level of importance. The importance of HOBr photolysis increases over time but remains minor. Although the reactions of HOBr are responsible for only a minor fraction of the bromine reduction in this case, the heterogenous reactions of HOBr are important for transferring bromine from HBr and HOBr to the more potent ozone destructive forms, and for generating the reactive chlorine involved in the BrO + ClO reactions.

The overall rate of ozone destruction within the plume is dependent upon the quantity of bromine cycling. As shown in Figure 9, compared to the 30th, bromine is transferred faster out of HBr and BrNO<sub>3</sub> on the 31st and 1st as these are denser (more concentrated) plumes with higher surface area density. Additionally, because several of the reactions listed in Table 4 are between halogen species originating from the volcanic emissions, they are faster in denser plumes. These factors result in a slower ozone destruction for 30th, as shown in Figure 15a. Because this ozone destruction is slower, but the plume travels faster, this difference is magnified if  $\Delta\text{O}_3/\text{SO}_2$  is plotted against distance (as is done in Figure 16).



#### 4.4.2 Comparison of model and aircraft data on ozone loss

Here we compare the aircraft observations to model outputs. Because the model plume does not precisely trace the same path as the observed plume, using the exact coordinates of each in-plume observation to identify the plume in the model domain would certainly often result in missing the modelled plume. Instead, for each of the plume encounters discussed in Sect. 3, we identify the equivalent of the observations in the model by the following method. Model data are considered "equivalent" for a plume encounter if they satisfy the following criteria:

- Time is closest to the median time of the observed encounter.
- Grid box is wholly or in part within the altitude range of the observed plume encounter.
- Grid box centre is within the range of distances from Etna for the observed plume encounter.
- SO<sub>2</sub> mixing ratio is in excess of 10 ppbv.

This effectively delimits a 3D space within the model. This 3D space is more likely to include the most concentrated part of the plume than the 1D transect made by the aircraft, and as such, the model data tends to include grid boxes with SO<sub>2</sub> greater than the maximum values from the observed plume encounter. For this reason our observation-model comparisons are based on O<sub>3</sub> vs. SO<sub>2</sub> trends rather than absolute values.

The model output is hourly, and the looping flight path (Figure 2) means that many of the plume encounters were made minutes apart at nearly the same points in space. As a result, several of these model-equivalent sets share many model data points and are nearly identical. Model equivalents of Figures 4 and 5 are shown, respectively, in Figures S7 and S8. The coefficients from simple linear regression of these data are tabulated in Table 5.

The gradients of  $\Delta\text{O}_3/\text{SO}_2$  versus plume age from applying a linear regression to the model and observation data are very similar. Weighting by the quantity and  $R^2$  of the fit of the observational data, the root mean square difference of the two gradients is 0.005, with a weighted mean bias of less than 0.001. Figure 16 plots modelled  $\Delta\text{O}_3/\text{SO}_2$  and these plume encounter gradients against distance from the volcano. The range of distances of the plume encounters is insufficient to determine any trend from the observations beyond those made in Sect. 3, however there is a reasonable match between observed and modelled  $\Delta\text{O}_3/\text{SO}_2$  values for distances of around 15 km from the volcano. This gives confidence that the model has skill with regards to the ozone chemistry of the plume.

The y-intercept of the lines of best fit in the model are consistently 15–20 ppbv lower than those of the observations, reflecting a somewhat higher background ozone. The cause of this is most likely bias in the initial and boundary conditions used in the model. We do not expect this offset to have a significant impact on the main results of this study, which are based on changes in ozone, ( $\Delta\text{O}_3$ ), rather than its absolute magnitude.

#### 4.4.3 Relationship of ozone losses to the magnitude of halogen emissions

As tabulated in Table 2, we ran the model with different volcanic fluxes in order to assess how volcanic impacts on ozone could vary for different passive degassing emission compositions. In Table 6 we report, for the *main*, *mag*, *hal*, and *oth* runs



#	Observation								Model		
	Day	time (UTC)	dur. /s	alt. / mASL	dist. / km	grad.	int. / ppbv	R <sup>2</sup>	grad.	int. / ppbv	R <sup>2</sup>
1	31	07:41:01–07:49:11	500	3596–3748	10.2–14.7	-0.020	47.1	0.20	-0.019	68.2	0.77
2	31	07:51:00–07:54:40	230	3699–3779	8.5–13.4	-0.011	48.6	0.53	-0.017	69.2	0.80
3	31	07:54:50–07:58:00	200	3700–3782	7.2–12.0	-0.006	49.2	0.06	-0.016	69.9	0.82
4	31	07:58:11–08:06:10	490	3555–3719	9.6–14.4	-0.025	51.9	0.44	-0.019	68.4	0.79
5	31	08:06:21–08:15:10	540	3466–3591	10.5–15.2	-0.016	50.0	0.50	-0.019	67.0	0.79
6	31	08:16:50–08:20:01	200	3484–3516	10.6–15.6	-0.022	50.4	0.51	-0.021	66.8	0.86
7	31	08:20:10–08:22:31	150	3466–3643	13.0–17.4	-0.007	46.9	0.19	-0.021	65.7	0.84
8	31	08:22:40–08:25:11	160	3567–3658	14.2–19.0	-0.023	48.1	0.71	-0.026	66.4	0.82
9	31	08:27:11–08:32:20	320	3597–3724	16.4–21.2	-0.025	48.5	0.80	-0.027	68.2	0.78
10	31	08:32:31–08:34:20	120	3623–3657	12.9–17.4	+0.009	42.1	0.23	-0.024	66.0	0.86
11	31	08:36:11–08:41:11	310	3604–3698	9.9–14.7	-0.003	43.4	0.16	-0.021	68.2	0.77
12	1	06:48:44–06:51:43	190	3090–3387	12.5–16.8	+0.006	49.2	0.11	-0.018	65.8	0.67
13	1	06:51:54–06:56:04	260	3430–3646	11.8–16.8	-0.019	51.0	0.54	-0.017	68.9	0.88
14	1	06:56:13–07:04:04	480	3486–3548	11.7–16.6	-0.017	50.4	0.65	-0.017	68.8	0.86
15	1	07:04:13–07:08:24	260	3506–3561	12.5–17.4	-0.015	50.9	0.81	-0.018	68.7	0.89
16	1	07:08:33–07:11:13	170	3510–3543	11.7–16.5	-0.020	51.7	0.67	-0.017	68.8	0.86
17	1	07:11:24–07:13:53	160	3490–3560	11.2–15.9	-0.014	48.8	0.91	-0.016	69.1	0.81
18	1	07:14:04–07:21:23	450	3420–3581	10.1–15.1	-0.019	51.2	0.75	-0.017	69.3	0.76
19	1	07:21:34–07:23:34	130	3249–3498	7.6–10.0	-0.046	53.4	0.97	-0.011	68.1	0.67

**Table 5.** Data relating to the major plume encounters, and the equivalent model data, depicted in Figures 4 and 5 (observations) and Figures S7 and S8 (model). dur = duration of plume encounter, alt = range of altitudes of plume encounter, dist = distance from Etna, grad = gradient of line-of-best fit of O<sub>3</sub> vs. SO<sub>2</sub> slope, int = y-intercept of this line

the average  $\Delta\text{O}_3$  values (compared to the *novolc* run) in ppbv for modelled plume aged  $60 \pm 5$  minutes at 2012-08-01 08:00 as a metric for the volcanic impact on ozone. Collectively, these runs explore a two-dimensional parameter space of variations in halogen and other emissions. In all runs the chlorine emission is scaled to the bromine emission (Cl/Br = 300 by mass), the bromine is emitted in the same 3:1 fixed proportions of HBr and Br, and all other species (H<sub>2</sub>O, Hg, OH, NO, at-source aerosol) are scaled to the SO<sub>2</sub> emission. In the absence of both SO<sub>2</sub> and bromine emissions the ozone loss relative to the *novolc* run is by definition zero. In the absence of halogens (only), the plume is slightly ozone productive, a phenomenon we ascribe to the impact of the NO emissions. Table 6 confirms that it is the halogen emission that causes the ozone loss.

Increasing the modelled flux of all species other than the halogens above that of the *main* case does not significantly change the depletion amounts. However, decreasing this flux by two-thirds limits ozone depletion by around 20%. As was the case for the 30th in the *main* model run, the surface area density is insufficient to quickly move bromine from HBr to the ozone-destructive cycle – though in this case this is due to weaker aerosol emissions rather than faster wind speeds.

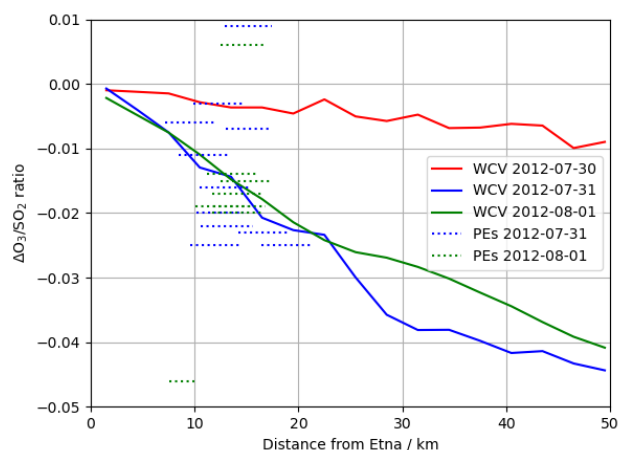


**Figure 16.** Modelled  $\Delta O_3/SO_2$  ratios at 0800 UTC on 2012-07-30, 2012-07-31, and 2012-07-31 (solid lines), and observed  $O_3$  vs.  $SO_2$  gradient from each of the major plume encounters (dashed lines), plotted against distance from the volcano. Observations are plotted as lines spanning the range of distances from the volcano at for the plume encounter.

	Bromine emissions $g\ s^{-1}$			
	0	10	30	45
0	0			
13		-1.1	-5.5	
40	0.6	-1.3	-7.2	-13.4
60			-7.3	-13.3

**Table 6.**  $\Delta O_3$  values (compared to *novolc* run) in ppbv for plume aged  $60 \pm 5$  minutes at 2012-08-01 08:00 for various model runs with varying emissions. For all runs the Cl/Br, Br/HBr, OH/ $SO_2$ , NO/ $SO_2$ ,  $H_2O/SO_2$ , Hg/ $SO_2$ , and aerosol/ $SO_2$  emission ratios remain the same as in *main*. The 40  $kg\ s^{-1}$  row and 30  $g\ s^{-1}$  column indicate the emission fluxes used in *main*.

The four data points for different bromine fluxes at 40  $kg\ SO_2\ s^{-1}$  can be fitted to a second order polynomial,  $(\Delta O_3)_{60min} = -3.5 \times 10^{-3}x^2 - 0.15x + 0.6$  ppbv, where  $x$  is the volcanic bromine flux in  $g\ s^{-1}$ . We interpret this combination of a second- and first-order terms to be the product of the complexities of the chemistry. The reactions that recycle BrO through reaction with other halogen oxide species would be expected to have rates approximately proportional to the square of the amount of halogens in the plume, while the rates of those that recycle HOBr, including those that generate reactive halogens from hydrogen halides, would vary approximately linearly with this quantity.

We caution against scaling these results to the plumes of large eruptions. Such plumes could have near-total depletion of ozone and/or  $HO_x$  and produce non-linear effects beyond the scope of this study. The halogen chemistry of large eruptions is being investigated using the WCV model and will be the focus of a future study.



To conclude this study on passively degassing plumes, we analyse the WCV model outputs to highlight how volcanic halogens also impact nitrogen and mercury species

#### 570 4.5 $\text{NO}_x$ , $\text{NO}_y$ , and nitrate aerosol

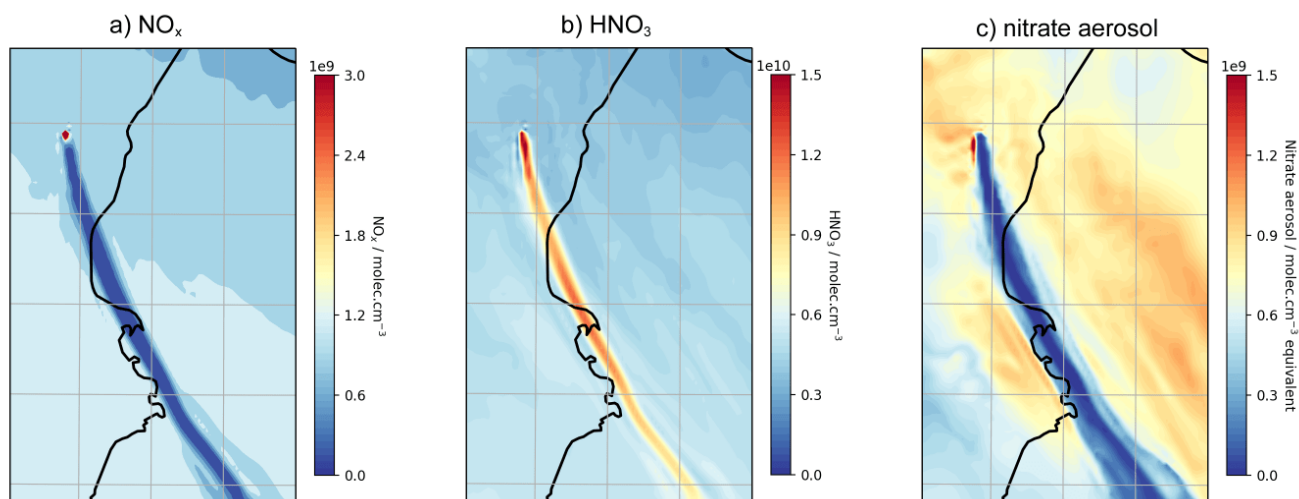


**Figure 17.** a) model mixing ratio of  $\text{NO}_x$ , b) model mixing ratio of  $\text{HNO}_3$ , c) equivalent mixing ratio of aerosol-phase nitrate at 3300mASL in the model at 0800 UTC on 2012-08-01.

Although the volcano degassing is a source of NO in the model, the plume is nearly totally depleted in  $\text{NO}_x$  (Figure 17a). The reason for plume  $\text{NO}_x$  being below background levels is the reaction sequence  $\text{BrO} + \text{NO}_2 \rightarrow \text{BrNO}_3$  followed by the heterogeneous reaction of  $\text{BrNO}_3$  with hydrogen halide that has the net effect of converting  $\text{NO}_2$  into  $\text{HNO}_3$ , a phenomenon discussed by Roberts et al. (2014). As a consequence, the plume is elevated in  $\text{HNO}_3$  compared to the background (17b).  
575 Elevated  $\text{HNO}_3$  has been observed in a number of volcanic plumes (Mather et al., 2004a, b; Martin et al., 2012; Voigt et al., 2014).

As well as the conversion of the volcanogenic and background  $\text{NO}_x$ , displacement of nitrate from background aerosol can also contribute to the in-plume  $\text{HNO}_3$ . The acidic plume, rich in sulfuric and hydrochloric acid, displaces nitrate from background aerosol into the gas phase as  $\text{HNO}_3$ . As shown in Figure 17c, the aerosol-phase nitrate content within the plume is  
580 much lower than the background in the model. The contributions of background  $\text{NO}_x$  (via  $\text{BrNO}_3$ ) and background nitrate (via acid displacement) to the plume  $\text{HNO}_3$  enhancement are of similar magnitude. In addition, conversion of volcanic  $\text{NO}_x$  (via  $\text{BrNO}_3$ ) into  $\text{HNO}_3$  contribute to further enhance the plume  $\text{HNO}_3$ .

As discussed by Martin et al. (2012) it is unclear from reaction kinetics if volcanoes are sources of reactive nitrogen. The levels of background  $\text{NO}_x$  and nitrate aerosol in the free-tropospheric environment modelled in this study (July-August 2012)  
585 would be too low to yield, by themselves,  $\text{HNO}_3$  concentrations of the order measured by (Mather et al., 2004a) at Mount



Etna summit in May 2002, nor those measured in the plume of Etna in a September 2011 aircraft campaign (Voigt et al., 2014). However background  $\text{NO}_x$  and nitrate may be significant contributors to volcanic  $\text{HNO}_3$  in more nitrogen-polluted environments. Voigt et al. (2014) states that typical conversion times of atmospheric  $\text{NO}_x$  to  $\text{HNO}_3$  is days in summer mid-latitudes, and so cannot explain formation of  $\text{HNO}_3$  in volcanic plumes. Our modelling results show in-plume gas-phase  $\text{HNO}_3$  being generated quickly by the mechanisms of acid displacement of background nitrate aerosol and volcanic plume halogen chemistry that converts background  $\text{NO}_x$  as well as volcanic  $\text{NO}_x$  (if present) into  $\text{HNO}_3$  via  $\text{BrNO}_3$ . These results suggest that analyses of  $\text{HNO}_3$  measurements within plumes used to assess volcanogenic  $\text{NO}_x$  or  $\text{NO}_y$  need to account for background reactive nitrogen in both the gas and particulate phases.

Due to the formation of the  $\text{BrNO}_3$  reservoir, a volcanic  $\text{NO}_x$  emission (or, potentially, background  $\text{NO}_x$  of similar magnitude to the plume bromine) could impact the bromine chemistry and speciation and limit the amount of reactive bromine available to form  $\text{BrO}$ . The quantity of  $\text{BrNO}_3$  that accumulates depends upon the abundance of  $\text{NO}_x$  available to react with  $\text{BrO}$  and the rate at which  $\text{BrNO}_3$  decays via heterogeneous chemistry. Of the three days modelled, only on the 30th, where the in-plume heterogeneous rates are low (due to a higher windspeed causing greater along-plume dilution), is a substantial fraction of plume bromine held in the  $\text{BrNO}_3$  reservoir for several minutes.

#### 4.6 Halogen impacts on mercury

The volcano is modelled to emit, per mol of  $\text{SO}_2$ ,  $7.8 \times 10^{-6}$  mol of Hg in an unoxidised state. A simplified Hg chemistry scheme has been implemented in WCV to evaluate the extent to which this Hg can become oxidised by interaction with the volcanic halogen halogen chemistry. Importantly, our mechanism includes the recently identified photo-reduction pathways of Hg(I)-halides (Saiz-Lopez et al., 2019). For the purposes of this study focused on halogens only, other possible mercury oxidation pathways are ignored. Due to the relatively low quantity of Hg in the plume, the effect of Hg on the halogen chemistry system itself is negligible.

Figure 18 shows the instantaneous average in-plume rates of reactions in the mercury cycle for plume aged 40-50 minutes at 2012-08-01 1200 UTC. Although there is a moderately fast oxidation of Hg to  $\text{HgBr}$  and  $\text{HgCl}$ , this is mostly offset by reduction. In agreement with global modeling of Saiz-Lopez et al. (2019), photolysis is the dominant Hg(I) reduction process. Overall, there is a small net oxidation of Hg occurring in the plume, but it is slow — for daytime plumes the average in-plume lifetime of  $\text{Hg}(0)$  is of the order of a few hours and this oxidation is mostly offset by photo-reduction. Despite the slow rate of oxidation in the plumes aged 10s of minutes, we find that in the early plume, modelled levels of mercury oxidation can be several % (Figure S6) from the first few minutes of evolution during both night and day. We attribute this oxidised mercury to oxidation occurring in the very early plume (first few seconds) where volcanogenic radicals are in high concentrations. This near instantaneous oxidation accounts for the vast majority of oxidised mercury in the modelled plume further downwind. Supporting this interpretation, we find negligible Hg oxidation in the first hour of plume evolution in output the *noHighT* run. Therefore variations in the Hg oxidation with plume age and time of day are due mostly the conditions at the point of emission, rather than any processes occurring within the downwind plume.



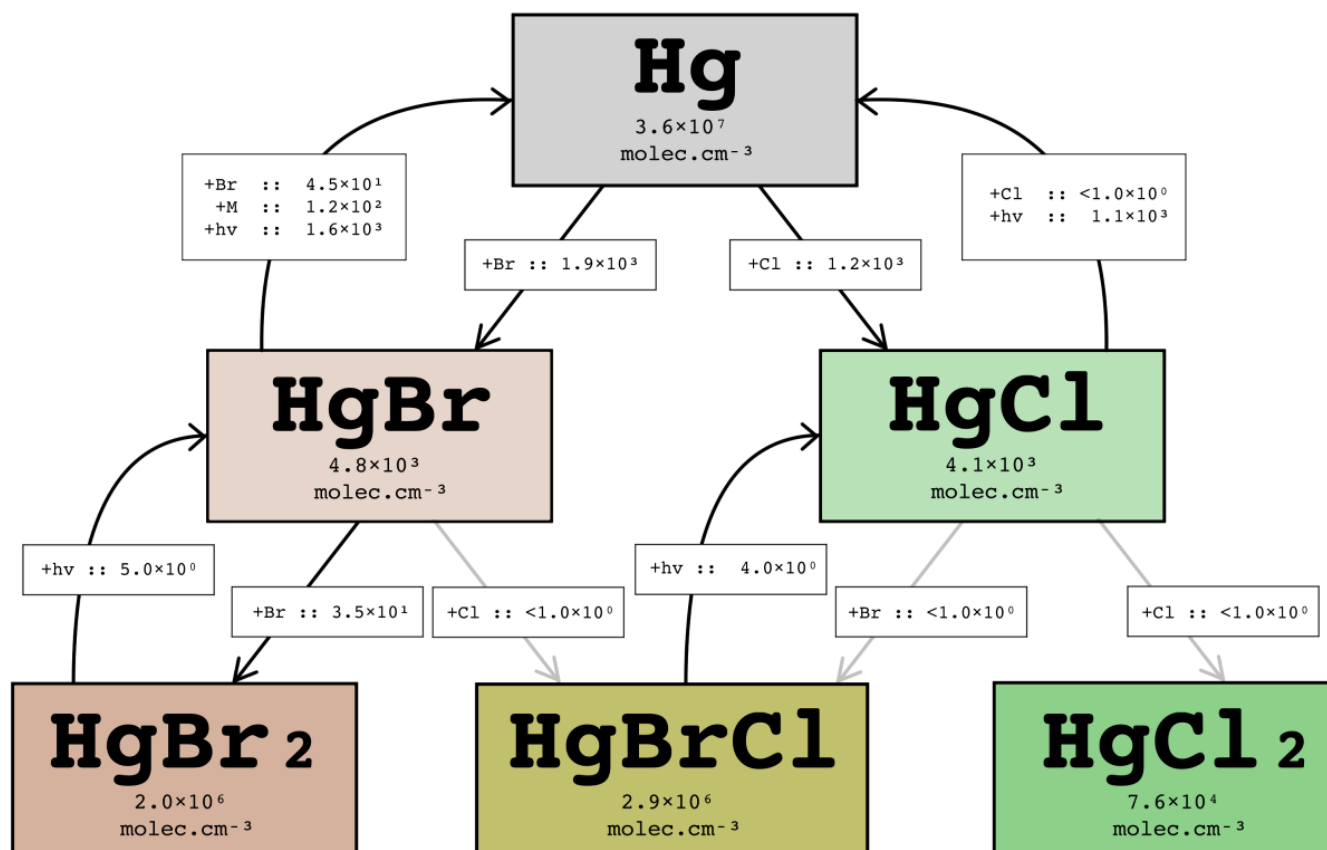


**Figure 18.** Instantaneous average in-plume concentrations and reaction rates (in molec cm<sup>-3</sup> s<sup>-1</sup>) for the Hg cycle for plume aged 40-50 minutes at 2012-08-01 1200 UTC. Rates less than 1 molec cm<sup>-3</sup> s<sup>-1</sup> are written as <1.0 × 10<sup>0</sup>.

We conclude that, for our case study of a Mount Etna passive degassing plume that focused on mercury-halogen interactions only, the net in-plume oxidation rate of mercury by halogen chemistry is near-negligible in the dispersed plume but could be significant very close to the source. Our findings contrast with the model study of von Glasow (2010) that predicted substantial oxidation of mercury to Hg(II) occurring in the dispersed volcanic plume of Mount Etna. However, that study did not include the very fast HgCl and HgBr photo-reduction pathways that critically impact the overall Hg oxidation, although it did include a SO<sub>2</sub>-mediated reduction of Hg(II) hypothesised by (Seigneur et al., 2006). We note that this slow net oxidation rate in the modelled evolved plume occurs despite the absence of this reduction pathway in the mechanism.

We invite caution regarding the interpretation of these results due to the very simple mercury chemical scheme used, and the apparent importance of the first few seconds of plume evolution which would be, spatially, poorly represented even at 1 km grid resolution.



630 Further investigation of mercury chemistry in volcanic plumes is needed, across a range of volcanic and meteorological conditions. This requires modeling at higher resolution to capture very near source processes both in the young cooled plume as well as investigations of hot plume chemistry just after emission, and the mercury chemistry in much larger eruption plumes that may differ from passive degassing case. The mercury oxidation-reduction scheme should also be extended to investigate possible roles of other gases (e.g.  $\text{NO}_x$ ). More comprehensive observation studies of speciated mercury at Mt. Etna and other volcanoes are also needed.

## 635 5 Conclusions

Volcanoes emit halogens that are converted into active chemical radicals in plumes and whose chemistry, notably bromine, causes ozone destruction. However, the plume processes driving this halogen conversion, the so-called halogen activation, and the ensuing ozone depletion within the volcanic plumes are not yet well constrained by the limited observational datasets and numerical model studies. It remains difficult to assess accurately the large-scale impact of volcanic halogens without a quantitative understanding of halogen plume chemistry. This study presents a new dataset of airborne measurements made during the summer 2012 in the degassing plume from the Mount Etna volcano, up to a few 10s of km from the source. This chemically reactive plume is simulated using a new numerical 3D model “WRF-Chem Volcano” (WCV), a version of WRF-Chem we have modified to incorporate volcanic emissions (including HBr and HCl) and multi-phase halogen chemistry.

640 Measurements of  $\text{SO}_2$  and ozone levels in the plume are found to be strongly anticorrelated. Ozone losses reach of up to about 10 ppbv. Accounting for the distance from the source at which these measurements were taken (7–21 km downwind from the summit), and using modelled wind speeds, the ozone destruction rate is estimated at approximately  $1.3 \times 10^{-5}$  mol  $\text{O}_3$  per mol  $\text{SO}_2$  per second. This value is similar to observation-derived estimates reported very close to the Mt Etna vents (<500 m downwind) (Surl et al., 2015), indicating continual ozone loss in the plume up to 10’s km downwind.

The aircraft observations are analysed with the WCV model forced by emission fluxes of volcanic gases, including  $\text{SO}_2$ , mercury, and halogens (HBr, HCl), each set to values within typical ranges observed for Etna in a passive degassing state. The model initialization also includes a representation of high-temperature radicals (Br, OH, NO) and a volcanic sulfate particle emission. The WCV mechanism includes photolytic, gas-phase and multi-phase reactions of bromine and chlorine, as well as gas-phase oxidation of  $\text{SO}_2$ . WCV was run using two-way nested grids, enabling 1 km resolution for the simulation of plume processes close to the volcano — the focus of this study.

655 The model simulates the in-plume conversion of emitted HBr into halogen radicals such as BrO, and ozone destruction in the volcanic plume. Modelled in-plume BrO/ $\text{SO}_2$  columns are similar to those observed at Mount Etna and other volcanoes, both in terms of magnitude (molar ratio of around  $10^{-4}$ ) and their spatial variation (rise and plateau with distance downwind). For modelled plume corresponding to the observations the resulting  $\text{O}_3$  versus  $\text{SO}_2$  gradients are very similar to those in the observational data. We compute  $\Delta\text{O}_3$ , the modelled ozone change due to the plume, by comparing output from model runs with and without volcanic emissions. The variation of  $\Delta\text{O}_3/\text{SO}_2$  ratios with plume age yields the rate of ozone loss as a ratio of  $\text{SO}_2$ . At the time of the plume measurements on 2012-08-01, this quantity is approximately  $7.5 \times 10^{-6}$  molec molec $^{-1}$  s $^{-1}$ ,



with a very similar value from an analysis of the instantaneous rates of reactions. In summary, the WCV model shows apparent skill in reproducing plume halogen chemistry and impacts on tropospheric ozone.

665 Inspecting the bromine chemical system, we found that HBr, the dominant form of bromine at emission, is converted to other forms within the first few minutes of plume evolution. These forms undergo a continuous cycling in the plume, with BrO and HOBr being the dominant daytime forms. We found that a lower plume density, caused by a greater wind speed, slowed the evolution of the bromine chemical system with more bromine residing in HBr, HOBr, and BrONO<sub>2</sub>. The balance between BrO and HOBr varies moderately with time of day due to diurnal variations in HO<sub>2</sub>, yielding slightly lower BrO/SO<sub>2</sub> around solar noon. Inspection of the rates of reaction find that although the overall proportions of bromine in different forms stabilises after 670 a few 10s of minutes of plume evolution, bromine is constantly cycling between forms, and this process includes the ozone destructive Br + O<sub>3</sub> → BrO reaction. Overall the ozone loss depends on several different reactions that reduce oxidised bromine without recreating ozone. We find that, for young plumes (<1 hour old), the most important reactions are those of BrO with halogen monoxides (BrO or ClO).

The conversion of volcanic HBr into reactive bromine forms occurs by the heterogeneous reaction of HOBr. Once plume HBr 675 is depleted, this reaction acts to convert HCl into reactive chlorine, leading to the release of methane-oxidising chlorine radicals. As a result the lifetime of methane is reduced in the plume core, however at the plume edge methane lifetime increases due to lower OH. The CH<sub>4</sub> oxidation initiates organic chemistry processing that results in formaldehyde being elevated in the plume compared to the background. Cl radicals also generate ClO and OClO — species that have also been detected in the plumes of some volcanoes including Mount Etna. Modelled near-source OClO/SO<sub>2</sub> ratios are of approximately similar magnitude (10<sup>-5</sup> 680 mol/mol) to those measured by Gliß et al. (2015).

The model plume chemistry is investigated over a range of emission scenarios. If the radical species expected to be produced in the high temperature volatile-air mix are excluded, the evolution of the halogen chemistry is greatly slowed and delayed. This result highlights the importance of understanding these very early processes in order to have an accurate picture of the overall chemistry. A sensitivity study of the model response to variations in the emissions of both halogens and sulfur finds 685 that ozone loss depends on the bromine emission flux with both linear and quadratic components, reflecting the complexities of the plume chemistry.

Finally, the model outputs are inspected to identify halogen impacts on HO<sub>x</sub>, sulfur, NO<sub>x</sub> and mercury chemistry.

Despite the volcano being an initial source of high-temperature OH radicals, for the early (<1 hr age) plume considered in this study the in-plume instantaneous lifetime of SO<sub>2</sub> in the model is substantially increased (from about 2 days to about 2 weeks) 690 due to depletion of OH. These modelling results therefore strengthen the case for using SO<sub>2</sub> as a plume tracer on these scales. The substantial depletion of OH is attributed to both SO<sub>2</sub> and halogen chemistry which further reduces OH concentrations within the plume. Halogen chemistry also causes depletion of HO<sub>2</sub>.

The SO<sub>2</sub> oxidation that does occur nevertheless produces sulfate aerosol mass and surface area within the plume. Secondary aerosol is formed more quickly in a simulation that excludes volcanic halogens. This result demonstrates that volcanic halogen 695 chemistry can critically influence sulfur oxidation processes, and emphasizes the need to include halogens in studies of volcanic sulfate aerosol impacts.



Despite the volcano being modelled as an initial source of high-T NO, modelled in-plume NO<sub>x</sub> levels are lower than the surrounding air due to plume chemistry destroying these species. In-plume HNO<sub>3</sub> was found to be elevated for two reasons: bromine chemistry converts NO<sub>x</sub> to HNO<sub>3</sub>, and background aerosol-phase nitrate is displaced into the gas phase by the acidic plume.

The model includes a very simple mercury scheme which includes photolysis reduction of mercury halides. In this passively degassing case, WCV predicts some early-stage oxidation of mercury by the initial high-temperature region Br radicals, but — in contrast to previous model studies for Mount Etna passive degassing — predicts a very slow net oxidation by halogens in the downwind plume. Further model-observation studies of volcanic mercury are warranted.

Overall, the WCV model appears to show reasonable skill in replicating observed in-plume phenomena of ozone loss specific to this case study and established downwind trends in BrO/SO<sub>2</sub> for minutes-old passive degassing plumes more generally. This skill gives credence to the assessments of the chemical processes occurring within the plume. WCV operated using nested-grids enables to reach 1 km resolution, however, we suggest caution in using results from the model for processes occurring at sub-km scale within the very early plume. This study investigated the chemical processes occurring in the passively degassing plume of Mount Etna. We caution against extrapolating these results to stronger (more dense) eruption plumes, as such plumes may experience phenomena out of scope of this study, such as near-total ozone depletion that perturbs the halogen chemistry. WCV is being applied in a follow-up study to investigate the plume chemical processes in such dense plumes from volcanic eruptions to the troposphere, as a contrast to this passive degassing case. In future, WCV can also be applied to assess the tropospheric impacts of volcanic halogen chemistry in plumes as they disperse and may remain chemically active for up to regional scales.

*Code availability.* Availability of model code

The code of WCV is available on GitHub (Surl, 2020). This repository is being actively maintained. The version of the code used to generate the results of this study are included in this repository as a static branch (etna2012).

The modifications to the PrepChem utility have been submitted to the maintainers of this software for consideration, and are available from the authors on request.

*Data availability.* Data availability

WRF-Chem generates NetCDF files as output. The output relating to the innermost domain (*d04* on Figure 3) are uploaded to a Zenodo online repository (Surl, 2021). This repository also contains the input settings files used for the runs.

*Author contributions.*



725 L.S. analysed the observational data, made the model code modifications, ran the model, and analysed and visualised the model output. All authors wrote the manuscript, provided critical feedback, and helped shape the research and analysis. T.R. supervised the project.

*Competing interests.*

The authors declare they have no competing interests.

730 *Acknowledgements.* This manuscript is a result of a project that has received funding from the European Union's Horizon 2020 research and innovation programme under grant agreement No 800062, as well as ANR Projet de Recherche Collaborative VOLC-HAL-CLIM (Volcanic Halogens: from Deep Earth to Atmospheric Impacts), ANR-18-CE01-0018.

Computer modeling benefited from access to IDRIS HPC resources (GENCI allocation A007017141) and the IPSL mesoscale computing center (CICLAD: Calcul Intensif pour le CLimat, l'Atmosphère et la Dynamique).

735 Aircraft measurements were carried out within the Global Mercury Observation System project (GMOS; [www.gmos.eu](http://www.gmos.eu)) and we acknowledge the contribution of the GMOS teams of CNR IIA, Italy and Helmholtz-Zentrum Geesthacht, Germany. GMOS was financially supported by the European Union within the seventh framework programme (FP-7, Project ENV.2010.4.1.3-2).

The authors would like to thank Louis Marelle and Jennie Thomas for their assistance with the model development. The model presented in this manuscript is a development on work undertaken as part of Luke Surl's PhD which was funded by the UK's Natural Environment

740 Research Council, and supervised by Deanna Donohoue and Roland von Glasow.



## References

- Aiuppa, A., Bellomo, S., D'Alessandro, W., Federico, C., Ferm, M., and Valenza, M.: Volcanic plume monitoring at Mount Etna by diffusive (passive) sampling, *Journal of Geophysical Research: Atmospheres*, 109, <https://doi.org/10.1029/2003JD004481>, 2004.
- 745 Aiuppa, A., Federico, C., Franco, A., Giudice, G., Gurrieri, S., Inguaggiato, S., Liuzzo, M., McGonigle, A. J. S., and Valenza, M.: Emission of bromine and iodine from Mount Etna volcano, *Geochemistry Geophysics Geosystems*, 6, <https://doi.org/10.1029/2005gc000965>, 2005.
- Aiuppa, A., Franco, A., von Glasow, R., Allen, A. G., D'Alessandro, W., Mather, T. A., Pyle, D. M., and Valenza, M.: The tropospheric processing of acidic gases and hydrogen sulphide in volcanic gas plumes as inferred from field and model investigations, *Atmospheric Chemistry and Physics*, 7, 1441–1450, <https://doi.org/10.5194/acp-7-1441-2007>, 2007.
- 750 Aiuppa, A., Giudice, G., Gurrieri, S., Liuzzo, M., Burton, M., Caltabiano, T., McGonigle, A. J. S., Salerno, G., Shinohara, H., and Valenza, M.: Total volatile flux from Mount Etna, *Geophysical Research Letters*, 35, <https://doi.org/10.1029/2008GL035871>, 2008.
- Badia, A., Reeves, C. E., Baker, A. R., Saiz-Lopez, A., Volkamer, R., Koenig, T. K., Apel, E. C., Hornbrook, R. S., Carpenter, L. J., Andrews, S. J., Sherwen, T., and von Glasow, R.: Importance of reactive halogens in the tropical marine atmosphere: a regional modelling study using WRF-Chem, *Atmospheric Chemistry and Physics*, 19, 3161–3189, <https://doi.org/10.5194/acp-19-3161-2019>, 2019.
- 755 Bagnato, E., Aiuppa, A., Parello, F., Calabrese, S., D'Alessandro, W., T.A., M., McGonigle, A., Pyle, D., and Wängberg, I.: Degassing of gaseous (elemental and reactive) and particulate mercury from Mount Etna volcano (Southern Italy), *Atmospheric Environment*, 41, 7377–7388, <https://doi.org/10.1016/j.atmosenv.2007.05.060>, 2007.
- Bagnato, E., Tamburello, G., Avard, G., Martinez Cruz, M., Enrico, M., Fu, X., Sprovieri, M., and Sonke, J.: Mercury fluxes from volcanic and geothermal sources: An update, *Geological Society London Special Publications*, 410, <https://doi.org/10.1144/SP410.2>, 2014.
- Bekki, S.: Oxidation of volcanic SO<sub>2</sub>: A sink for stratospheric OH and H<sub>2</sub>O, *Geophysical Research Letters*, 22, 913–916, <https://doi.org/10.1029/95gl00534>, 1995.
- 760 Bobrowski, N. and Giuffrida, G.: Bromine monoxide / sulphur dioxide ratios in relation to volcanological observations at Mt. Etna 2006–2009, *Solid Earth*, 3, 433–445, <https://doi.org/10.5194/se-3-433-2012>, 2012.
- Bobrowski, N., Hönninger, G., Galle, B., and Platt, U.: Detection of bromine monoxide in a volcanic plume, *Nature*, 423, 273–276, <https://doi.org/10.1038/nature01625>, 2003.
- 765 Bobrowski, N., von Glasow, R., Aiuppa, A., Inguaggiato, S., Louban, I., Ibrahim, O. W., and Platt, U.: Reactive halogen chemistry in volcanic plumes, *Journal of Geophysical Research-Atmospheres*, 112, <https://doi.org/10.1029/2006jd007206>, 2007.
- Bobrowski, N., von Glasow, R., Giuffrida, G. B., Tedesco, D., Aiuppa, A., Yalire, M., Arellano, S., Johansson, M., and Galle, B.: Gas emission strength and evolution of the molar ratio of BrO/SO<sub>2</sub> in the plume of Nyiragongo in comparison to Etna, *Journal of Geophysical Research: Atmospheres*, 120, 277–291, <https://doi.org/10.1002/2013jd021069>, 2015.
- 770 Bobrowski, N., Giuffrida, G. B., Arellano, S., Yalire, M., Liotta, M., Brusca, L., Calabrese, S., Scaglione, S., Rüdiger, J., Castro, J. M., Galle, B., and Tedesco, D.: Plume composition and volatile flux of Nyamulagira volcano, Democratic Republic of Congo, during birth and evolution of the lava lake, 2014–2015, *Bulletin of Volcanology*, 79, <https://doi.org/10.1007/s00445-017-1174-0>, 2017.
- Brenna, H., Kutterolf, S., Mills, M. J., and Krüger, K.: The potential impacts of a sulfur- and halogen-rich supereruption such as Los Chocoyos on the atmosphere and climate, *Atmospheric Chemistry and Physics*, 20, 6521–6539, <https://doi.org/10.5194/acp-20-6521-2020>, 2020.
- 775 Buchholz, R. R., Emmons, L. K., Tilmes, S., and The CESM2 Development Team: CESM2.1/CAM-chem Instantaneous Output for Boundary Conditions - Subset used: 20°N–45°N, 5°E–45°E 2018-12-21–2018-12-29, Accessed: 10-12-2019, <https://doi.org/10.5065/NMP7-EP60>, <https://wiki.ucar.edu/display/camchem/CESM2.1:CAM-chem+as+Boundary+Conditions>, 2019.



- Cadoux, A., Scaillet, B., Bekki, S., Oppenheimer, C., and Druitt, T. H.: Stratospheric Ozone destruction by the Bronze-Age Minoan eruption (Santorini Volcano, Greece), *Scientific Reports*, 5, <https://doi.org/10.1038/srep12243>, 2015.
- 780 Dinger, F., Bobrowski, N., Warnach, S., Bredemeyer, S., Hidalgo, S., Arellano, S., Galle, B., Platt, U., and Wagner, T.: Periodicity in the BrO/SO<sub>2</sub> molar ratios in the volcanic gas plume of Cotopaxi and its correlation with the Earth tides during the eruption in 2015, *Solid Earth*, 9, 247–266, <https://doi.org/10.5194/se-9-247-2018>, 2018.
- Emmons, L. K., Schwantes, R. H., Orlando, J. J., Tyndall, G., Kinnison, D., Lamarque, J.-F., Marsh, D., Mills, M. J., Tilmes, S., Bardeen, C., Buchholz, R. R., Conley, A., Gettelman, A., Garcia, R., Simpson, I., Blake, D. R., Meinardi, S., and Pétron, G.: The Chemistry Mechanism  
785 in the Community Earth System Model version 2 (CESM2), *Journal of Advances in Modeling Earth Systems*, p. e2019MS001882, 2020.
- Freitas, S. R., Longo, K. M., Alonso, M. F., Pirre, M., Marecal, V., Grell, G., Stockler, R., Mello, R. F., and Sánchez Gácita, M.: PREP-CHEM-SRC – 1.0: a preprocessor of trace gas and aerosol emission fields for regional and global atmospheric chemistry models, *Geoscientific Model Development*, 4, 419–433, <https://doi.org/10.5194/gmd-4-419-2011>, 2011.
- Galeazzo, T., Bekki, S., Martin, E., Savarino, J., and Arnold, S. R.: Photochemical box modelling of volcanic SO<sub>2</sub> oxidation: isotopic  
790 constraints, *Atmospheric Chemistry and Physics*, 18, 17 909–17 931, <https://doi.org/10.5194/acp-18-17909-2018>, 2018.
- General, S., Bobrowski, N., Pöhler, D., Weber, K., Fischer, C., and Platt, U.: Airborne I-DOAS measurements at Mt. Etna: BrO and OCIO evolution in the plume, *Journal of Volcanology and Geothermal Research*, <https://doi.org/10.1016/j.jvolgeores.2014.05.012>, in press, 2014.
- Gerlach, T. M.: Volcanic sources of tropospheric ozone-depleting trace gases, *Geochemistry Geophysics Geosystems*, 5, <https://doi.org/10.1029/2004gc000747>, 2004.
- 795 Gliß, J., Bobrowski, N., Vogel, L., Pöhler, D., and Platt, U.: OCIO and BrO observations in the volcanic plume of Mt. Etna – implications on the chemistry of chlorine and bromine species in volcanic plumes, *Atmospheric Chemistry and Physics*, 15, 5659–5681, <https://doi.org/10.5194/acp-15-5659-2015>, 2015.
- Grell, G. A., Peckham, S. E., Schmitz, R., McKeen, S. A., Frost, G., Skamarock, W. C., and Eder, B.: Fully coupled “online” chemistry within the WRF model, *Atmospheric Environment*, 39, 6957–6975, <https://doi.org/10.1016/j.atmosenv.2005.04.027>, 2005.
- 800 Gutmann, A., Bobrowski, N., Roberts, T. J., Rüdiger, J., and Hoffmann, T.: Advances in Bromine Speciation in Volcanic Plumes, *Frontiers in Earth Science*, 6, 213, <https://doi.org/10.3389/feart.2018.00213>, 2018.
- Hörmann, C., Sihler, H., Bobrowski, N., Beirle, S., Penning de Vries, M., Platt, U., and Wagner, T.: Systematic investigation of bromine monoxide in volcanic plumes from space by using the GOME-2 instrument, *Atmospheric Chemistry and Physics*, 13, 4749–4781, <https://doi.org/10.5194/acp-13-4749-2013>, 2013.
- 805 Jourdain, L., Roberts, T. J., Pirre, M., and Josse, B.: Modeling the reactive halogen plume from Ambrym and its impact on the troposphere with the CCATT-BRAMS mesoscale model, *Atmospheric Chemistry and Physics*, 16, 12 099–12 125, <https://doi.org/10.5194/acp-16-12099-2016>, <https://www.atmos-chem-phys.net/16/12099/2016/>, 2016.
- Kelly, P. J., Kern, C., Roberts, T. J., Lopez, T., Werner, C., and Aiuppa, A.: Rapid chemical evolution of tropospheric volcanic emissions from Redoubt Volcano, Alaska, based on observations of ozone and halogen-containing gases, *Journal of Volcanology and Geothermal  
810 Research*, 259, 317–333, <https://doi.org/10.1016/j.jvolgeores.2012.04.023>, 2013.
- Kutterolf, S., Hansteen, T., Appel, K., Freundt, A., Kröger, K., Pérez, W., and Wehrmann, H.: Combined bromine and chlorine release from large explosive volcanic eruptions: A threat to stratospheric ozone?, *Geology*, 41, 707–710, <https://doi.org/10.1130/G34044.1>, 2013.
- Lurton, T., Jégou, F., Berthet, G., Renard, J.-B., Clarisse, L., Schmidt, A., Brogniez, C., and Roberts, T. J.: Model simulations of the chemical and aerosol microphysical evolution of the Sarychev Peak 2009 eruption cloud compared to in situ and satellite observations, *Atmospheric  
815 Chemistry and Physics*, 18, 3223–3247, <https://doi.org/10.5194/acp-18-3223-2018>, 2018.



- Marelle, L., Thomas, J. L., Ahmed, S., Tuite, K., Stutz, J., Dommergue, A., Simpson, W. R., and Frey, M. M.: Implementation and impacts of surface and blowing snow sources of Arctic bromine activation within WRF-Chem, *Journal of Advances in Modeling Earth Systems*, in review.
- Martin, R. S., Ilyinskaya, E., and Oppenheimer, C.: The enigma of reactive nitrogen in volcanic emissions, *Geochimica et Cosmochimica Acta*, 95, 93–105, <https://doi.org/10.1016/j.gca.2012.07.027>, 2012.
- 820 Maters, E. C., Delmelle, P., Rossi, M. J., and Ayriss, P. M.: Reactive Uptake of Sulfur Dioxide and Ozone on Volcanic Glass and Ash at Ambient Temperature, *Journal of Geophysical Research: Atmospheres*, 122, 10,077–10,088, <https://doi.org/10.1002/2017JD026993>, 2017.
- Mather, T., Allen, A., Davison, B., Pyle, D., Oppenheimer, C., and McGonigle, A.: Nitric acid from volcanoes, *Earth and Planetary Science Letters*, 218, 17 – 30, [https://doi.org/10.1016/S0012-821X\(03\)00640-X](https://doi.org/10.1016/S0012-821X(03)00640-X), 2004a.
- 825 Mather, T. A., Pyle, D. M., and Allen, A. G.: Volcanic source for fixed nitrogen in the early Earth's atmosphere, *Geology*, 32, 905–908, <https://doi.org/10.1130/G20679.1>, 2004b.
- Millard, G. A., Mather, T. A., Pyle, D. M., Rose, W. I., and Thornton, B.: Halogen emissions from a small volcanic eruption: Modeling the peak concentrations, dispersion, and volcanically induced ozone loss in the stratosphere, *Geophysical Research Letters*, 33, 830 <https://doi.org/10.1029/2006GL026959>, 2006.
- National Centers for Environmental Prediction, National Weather Service, NOAA, and U.S. Department of Commerce: NCEP FNL Operational Model Global Tropospheric Analyses, continuing from July 1999 - accessed 2019, <https://doi.org/10.5065/D6M043C6>, 2000.
- Oppenheimer, C., Kyle, P., Eisele, F., Crawford, J., Huey, G., Tanner, D., Kim, S., Mauldin, L., Blake, D., Beyersdorf, A., Buhr, M., and Davis, D.: Atmospheric chemistry of an Antarctic volcanic plume, *Journal of Geophysical Research-Atmospheres*, 115, 835 <https://doi.org/10.1029/2009jd011910>, 2010.
- Oppenheimer, C., Scaillet, B., and Martin, R. S.: Sulfur Degassing From Volcanoes: Source Conditions, Surveillance, Plume Chemistry and Earth System Impacts, *Reviews in Mineralogy and Geochemistry*, 73, 363–421, <https://doi.org/10.2138/rmg.2011.73.13>, 2011.
- Pyle, D. and Mather, T.: Halogens in igneous processes and their fluxes to the atmosphere and oceans from volcanic activity: A review, *Chemical Geology*, 263, 110–121, <https://doi.org/10.1016/j.chemgeo.2008.11.013>, 2009.
- 840 Pyle, D. M. and Mather, T. A.: The importance of volcanic emissions for the global atmospheric mercury cycle, *Atmospheric Environment*, 37, 5115 – 5124, <https://doi.org/10.1016/j.atmosenv.2003.07.011>, 2003.
- Roberts, T.: Ozone Depletion in Tropospheric Volcanic Plumes: From Halogen-Poor to Halogen-Rich Emissions, *Geosciences*, 8, 68, <https://doi.org/10.3390/geosciences8020068>, 2018.
- Roberts, T., Vignelles, D., Liuzzo, M., Giudice, G., Aiuppa, A., Coltelli, M., Salerno, G., Chartier, M., Couté, B., Berthet, G., Lurton, T., 845 Dulac, F., and Renard, J.-B.: The primary volcanic aerosol emission from Mt Etna: Size-resolved particles with SO<sub>2</sub> and role in plume reactive halogen chemistry, *Geochimica et Cosmochimica Acta*, 222, 74–93, <https://doi.org/10.1016/j.gca.2017.09.040>, 2018.
- Roberts, T., Dayma, G., and Oppenheimer, C.: Reaction Rates Control High-Temperature Chemistry of Volcanic Gases in Air, *Frontiers in Earth Science*, 7, 154, <https://doi.org/10.3389/feart.2019.00154>, 2019.
- Roberts, T. J., Braban, C. F., Martin, R. S., Oppenheimer, C., Adams, J. W., Cox, R. A., Jones, R. L., and Griffiths, 850 P. T.: Modelling reactive halogen formation and ozone depletion in volcanic plumes, *Chemical Geology*, 263, 151–163, <https://doi.org/10.1016/j.chemgeo.2008.11.012>, 2009.





- Roberts, T. J., Martin, R. S., and Jourdain, L.: Reactive bromine chemistry in Mount Etna's volcanic plume: the influence of total Br, high-temperature processing, aerosol loading and plume-air mixing, *Atmospheric Chemistry and Physics*, 14, 11 201–11 219, <https://doi.org/10.5194/acp-14-11201-2014>, 2014.
- 855 Rose, W. I., Millard, G. A., Mather, T. A., Hunton, D. E., Anderson, B., Oppenheimer, C., Thornton, B. F., Gerlach, T. M., Viggiano, A. A., Kondo, Y., Miller, T. M., and Ballenthin, J. O.: Atmospheric chemistry of a 33–34 hour old volcanic cloud from Hekla Volcano (Iceland): Insights from direct sampling and the application of chemical box modeling, *Journal of Geophysical Research*, 111, <https://doi.org/10.1029/2005jd006872>, 2006.
- 860 Rüdiger, J., Bobrowski, N., Liotta, M., and Hoffmann, T.: Development and application of a sampling method for the determination of reactive halogen species in volcanic gas emissions, *Analytical and Bioanalytical Chemistry*, 409, 5975–5985, <https://doi.org/10.1007/s00216-017-0525-1>, 2017.
- Rüdiger, J., Gutmann, A., Bobrowski, N., Liotta, M., de Moor, J. M., Sander, R., Dinger, F., Tirpitz, J.-L., Ibarra, M., Saballos, A., Martínez, M., Mendoza, E., Ferrufino, A., Stix, J., Valdés, J., Castro, J. M., and Hoffmann, T.: Halogen activation in the plume of Masaya volcano: field observations and box model investigations, *Atmospheric Chemistry and Physics Discussions*, <https://doi.org/10.5194/acp-2020-284>,  
865 2020.
- Saiz-Lopez, A., Sitkiewicz, S. P., Roca-Sanjuán, D., Oliva-Enrich, J. M., Dávalos, J. Z., Notario, R., Jiskra, M., Xu, Y., Wang, F., Thackray, C. P., Sunderland, E. M., Jacob, D. J., Travnikov, O., Cuevas, C. A., Acuña, A. U., Rivero, D., Plane, J. M. C., Kinnison, D. E., and Sonke, J. E.: Photoreduction of gaseous oxidized mercury changes global atmospheric mercury speciation, transport and deposition, *Nature Communications*, 9, <https://doi.org/10.1038/s41467-018-07075-3>, 2018.
- 870 Saiz-Lopez, A., Acuña, A. U., Trabelsi, T., Carmona-García, J., Dávalos, J. Z., Rivero, D., Cuevas, C. A., Kinnison, D. E., Sitkiewicz, S. P., Roca-Sanjuán, D., and Francisco, J. S.: Gas-Phase Photolysis of Hg(I) Radical Species: A New Atmospheric Mercury Reduction Process, *Journal of the American Chemical Society*, 141, 8698–8702, <https://doi.org/10.1021/jacs.9b02890>, 2019.
- Salerno, G., Burton, M., Oppenheimer, C., Caltabiano, T., Randazzo, D., Bruno, N., and Longo, V.: Three-years of SO<sub>2</sub> flux measurements of Mt. Etna using an automated UV scanner array: Comparison with conventional traverses and uncertainties in flux retrieval, *Journal of*  
875 *Volcanology and Geothermal Research*, 183, 76–83, <https://doi.org/10.1016/j.jvolgeores.2009.02.013>, 2009.
- Seigneur, C. and Lohman, K.: Effect of bromine chemistry on the atmospheric mercury cycle, *Journal of Geophysical Research: Atmospheres*, 113, D23309, <https://doi.org/10.1029/2008JD010262>, 2008.
- Seigneur, C., Vijayaraghavan, K., and Lohman, K.: Atmospheric mercury chemistry: Sensitivity of global model simulations to chemical reactions, *Journal of Geophysical Research*, 111, D22306, <https://doi.org/10.1029/2005jd006780>, 2006.
- 880 Seo, S., Richter, A., Blechschmidt, A.-M., Bougoudis, I., and Burrows, J. P.: First high-resolution BrO column retrievals from TROPOMI, *Atmospheric Measurement Techniques*, 12, 2913–2932, <https://doi.org/10.5194/amt-12-2913-2019>, 2019.
- Surl, L.: Modelling the atmospheric chemistry of volcanic plumes, Ph.D. thesis, University of East Anglia, <https://ueaeprints.uea.ac.uk/id/eprint/59407/>, 2016.
- Surl, L.: WRF-Chem Volcano [software], <https://github.com/LukeSurl/WCV>, 2020.
- 885 Surl, L.: WRF-Chem Volcano output - Etna Summer 2012 [dataset], <https://doi.org/10.5281/zenodo.4415788>, 2021.
- Surl, L., Donohoue, D., Aiuppa, A., Bobrowski, N., and von Glasow, R.: Quantification of the depletion of ozone in the plume of Mount Etna, *Atmospheric Chemistry and Physics*, 15, 2613–2628, <https://doi.org/10.5194/acp-15-2613-2015>, 2015.
- Vance, A., McGonigle, A. J. S., Aiuppa, A., Stith, J. L., Turnbull, K., and von Glasow, R.: Ozone depletion in tropospheric volcanic plumes, *Geophysical Research Letters*, 37, <https://doi.org/10.1029/2010GL044997>, 2010.



- 890 Voigt, C., Jessberger, P., Jurkat, T., Kaufmann, S., Baumann, R., Schlager, H., Bobrowski, N., Giuffrida, G., and Salerno, G.: Evolution of CO<sub>2</sub>, SO<sub>2</sub>, HCl, and HNO<sub>3</sub> in the volcanic plumes from Etna, *Geophysical Research Letters*, 41, 2196–2203, <https://doi.org/10.1002/2013gl058974>, 2014.
- von Glasow, R.: Atmospheric chemistry in volcanic plumes, *Proceedings of the National Academy of Sciences*, 107, 6594–6599, <https://doi.org/10.1073/pnas.0913164107>, 2010.
- 895 von Glasow, R., Bobrowski, N., and Kern, C.: The effects of volcanic eruptions on atmospheric chemistry, *Chemical Geology*, 263, 131–142, <https://doi.org/10.1016/j.chemgeo.2008.08.020>, 2009.
- Warnach, S., Bobrowski, N., Hidalgo, S., Arellano, S., Sihler, H., Dinger, F., Lübcke, P., Battaglia, J., Steele, A., Galle, B., Platt, U., and Wagner, T.: Variation of the BrO/SO<sub>2</sub> Molar Ratio in the Plume of Tungurahua Volcano Between 2007 and 2017 and Its Relationship to Volcanic Activity, *Frontiers in Earth Science*, 7, <https://doi.org/10.3389/feart.2019.00132>, <https://doi.org/10.3389/feart.2019.00132>, 2019.
- 900 Weigelt, A., Ebinghaus, R., Pirrone, N., Bieser, J., Bödewadt, J., Esposito, G., Slemr, F., van Velthoven, P. F. J., Zahn, A., and Ziereis, H.: Tropospheric mercury vertical profiles between 500 and 10,000 m in central Europe, *Atmospheric Chemistry and Physics*, 16, 4135–4146, <https://doi.org/10.5194/acp-16-4135-2016>, 2016a.
- Weigelt, A., Slemr, F., Ebinghaus, R., Pirrone, N., Bieser, J., Bödewadt, J., Esposito, G., and van Velthoven, P. F. J.: Mercury emissions of a coal-fired power plant in Germany, *Atmospheric Chemistry and Physics*, 16, 13 653–13 668, <https://doi.org/10.5194/acp-16-13653-2016>,  
905 2016b.
- Wennberg, P.: Atmospheric chemistry - Bromine explosion, *Nature*, 397, 299, <https://doi.org/10.1038/16805>, 1999.
- Wild, O., Zhu, X., and Prather, M. J.: Fast-J: Accurate Simulation of In- and Below-Cloud Photolysis in Tropospheric Chemical Models, *Journal of Atmospheric Chemistry*, 37, 245–282, <https://doi.org/10.1023/a:1006415919030>, 2000.
- Witt, M. L. I., Mather, T. A., Pyle, D. M., Aiuppa, A., Bagnato, E., and Tsanev, V. I.: Mercury and halogen emissions from Masaya and  
910 Telica volcanoes, Nicaragua, *Journal of Geophysical Research: Solid Earth*, 113, <https://doi.org/10.1029/2007JB005401>, 2008.
- Wittmer, J., Bobrowski, N., Liotta, M., Giuffrida, G., Calabrese, S., and U., P.: Active alkaline traps to determine acidic-gas ratios in volcanic plumes: sampling technique and analytical Methods, *Geochem. Geophys. Geosyst*, <https://doi.org/10.1002/2013GC005133>, 2014.
- Zaveri, R. A. and Peters, L. K.: A new lumped structure photochemical mechanism for large-scale applications, *Journal of Geophysical Research: Atmospheres*, 104, 30 387–30 415, <https://doi.org/10.1029/1999JD900876>, 1999.
- 915 Zaveri, R. A., Easter, R. C., Fast, J. D., and Peters, L. K.: Model for Simulating Aerosol Interactions and Chemistry (MOSAIC), *Journal of Geophysical Research: Atmospheres*, 113, <https://doi.org/10.1029/2007JD008782>, 2008.